Report Documentation Page

Form Approved
OMB No. 0704-0188

1. REPORT DATE	2. REPORT TYPE	3. DATES COVERED
17 JAN 2013	**Final**	**29-07-2010 to 29-07-2012**

4. TITLE AND SUBTITLE	5a. CONTRACT NUMBER
Average power and brightness scaling of diamond Raman lasers	**FA23861014078**
	5b. GRANT NUMBER
	5c. PROGRAM ELEMENT NUMBER
6. AUTHOR(S)	5d. PROJECT NUMBER
Richard Mildren	5e. TASK NUMBER
	5f. WORK UNIT NUMBER
7. PERFORMING ORGANIZATION NAME(S) AND ADDRESS(ES)	8. PERFORMING ORGANIZATION REPORT NUMBER
Macquarie University,NSW 2109,NSW, Australia,Australia,AU,2109	**N/A**
9. SPONSORING/MONITORING AGENCY NAME(S) AND ADDRESS(ES)	10. SPONSOR/MONITOR'S ACRONYM(S)
AOARD, UNIT 45002, APO, AP, 96338-5002	**AOARD**
	11. SPONSOR/MONITOR'S REPORT NUMBER(S)
	AOARD-104078

12. DISTRIBUTION/AVAILABILITY STATEMENT
Approved for public release; distribution unlimited

13. SUPPLEMENTARY NOTES

14. ABSTRACT

Diamond holds substantial promise as a high Raman gain laser material with outstanding power handling capability, yet despite this the highest reported output power from a diamond Raman laser prior to this project was approximately 1 W. This report describes investigations into order‐of‐magnitude power scaling of diamond Raman lasers. The investigations focus on 1064 nm beam conversion of 50 W lasers in the ?external cavity? Raman cavity configuration in both pulsed and continuous wave modes of operation. For pulsed operation, output powers up to 16 W are demonstrated with 40‐50% conversion efficiency from a compact acousto‐optically Q‐switched neodymium pump laser. The output power is similar to the highest achieved by other groups (in diamond and other Raman materials) but with much greater efficiency and using a much simpler overall system. More than 13 W is also demonstrated at the second‐Stokes wavelength at 1.49 micron in the so‐called eye‐safe region, a result which compares well in terms of efficiency as well as power with alternative leading high pulse rate eye‐safe laser technologies. The model‐backed experiments suggest thermal effects are negligible at the current power levels, and much higher output powers are likely when using high power pumps. For CW operation, output powers up to 16 W are demonstrated with conversion efficiency up to 40%. Efficiencies more closely approaching the quantum limit (86%) may be enabled by future improvements in diamond quality. As far as we are aware these are the first demonstrations of CW Raman conversion in a discrete all‐solid‐state system at multi‐watt powers. We show that the concept is applicable for output powers up to several hundred watts and holds promise as a widely applicable technology for high power CW conversion. We also report findings of a UV etching mechanism for diamond surfaces. This multi‐photon effect will need to be considered when using short wavelength pumps but may also provide a novel direct‐write method for creating high resolution structures such as laser waveguides.

15. SUBJECT TERMS

16. SECURITY CLASSIFICATION OF:			17. LIMITATION OF ABSTRACT	18. NUMBER OF PAGES	19a. NAME OF RESPONSIBLE PERSON
a. REPORT	b. ABSTRACT	c. THIS PAGE			
unclassified	**unclassified**	**unclassified**	**Same as Report (SAR)**	**32**	

Final Report for AOARD Grant 104078

"**Average power and brightness scaling of diamond Raman lasers**"

7 Jan 2012

Principal Investigator:
A/Prof Rich Mildren
rich.mildren@mq.edu.au
Macquarie University

Mailing Address:
Department of Physics and Astronomy,
Macquarie University, NSW, 2109 Australia

Phone: +61 2 9850 8965
Fax: +61 2 9850 8911

Period of Performance: Nov 10 – Nov 12

Abstract:
Most important research results that explain why the work was done, what was accomplished, and how it pushed scientific frontiers or advanced the field.

Diamond holds substantial promise as a high Raman gain laser material with outstanding power handling capability, yet despite this the highest reported output power from a diamond Raman laser prior to this project was approximately 1 W. This report describes investigations into order-of-magnitude power scaling of diamond Raman lasers. The investigations focus on 1064 nm beam conversion of 50 W lasers in the "external cavity" Raman cavity configuration in both pulsed and continuous wave modes of operation.

For pulsed operation, output powers up to 16 W are demonstrated with 40-50% conversion efficiency from a compact acousto-optically Q-switched neodymium pump laser. The output power is similar to the highest achieved by other groups (in diamond and other Raman materials) but with much greater efficiency and using a much simpler overall system. More than 13 W is also demonstrated at the second-Stokes wavelength at 1.49 μm in the so-called eye-safe region, a result which compares well in terms of efficiency as well as power with alternative leading high pulse rate eye-safe laser technologies. The model-backed experiments suggest thermal effects are negligible at the current power levels, and much higher output powers are likely when using high power pumps.

For continuous wave operation, output powers up to 16 W are demonstrated with conversion efficiency up to 40%. Efficiencies more closely approaching the quantum limit (86%) may be enabled by future improvements in diamond quality. As far as we are aware these are the first demonstrations of CW Raman conversion in a discrete all-solid-state system at multi-watt powers. We show that the concept is applicable for output powers up to several hundred watts and holds promise as a widely applicable technology for high power CW conversion.

We also report findings of a UV etching mechanism for diamond surfaces. This multi-photon effect will need to be considered when using short wavelength pumps but may also provide a novel direct-write method for creating high resolution structures such as laser waveguides.

Introduction:
Summary of specific aims of the research and describe the importance and ultimate goal of the work.

Although diamond is well known as an excellent Raman material, the emergence of diamond Raman lasers as practical devices has emerged only recently with the production of low absorption Type IIa diamond using the growth method of chemical vapor deposition. Prior to the start of this project in 2009, my team had first demonstrated synthetic diamond Raman lasers and reported conversion efficiencies higher than that observed in any other crystalline material. This initial work was performed at average output powers of approximately 1.2-Watts. This project aims to leverage diamond's extraordinary thermal properties to demonstrate Raman laser devices at much higher average powers.

The specific aims are to:

- Assess in detail of the potential for diamond Raman lasers to provide wavelength and brightness conversion of mature one micron laser technologies.
- Establish design rules for scaling towards kilowatt power levels.

These aims were addressed by investigating pulsed and continuous wave diamond Raman laser systems using Nd laser pumps at powers up to 50 W. Power scaling and limiting factors were investigated by analyzing system performance and accompanying model simulations.

This work is important in that it explores an active laser material with the highest, by a large margin, known room temperature thermal conductivity as well as a host of other thermal advantages. The research is therefore of potentially fundamental importance for developing compact high-power wavelength and brightness converters that minimize deleterious thermal effects on important performance metrics such as efficiency and brightness. The resulting devices may provide major advantages in wavelength-choice and/or brightness over alternative technologies such as optical parametric oscillators and Raman shifters based on non-diamond materials, and comprise a suitable platform for Raman beam combination with high average output power.

Experiment:
Description of the experiment(s)/theory and equipment or analyses.

The experiments can be conveniently divided into two streams of investigation: Pulsed and continuous wave (CW) diamond Raman lasers (DRLs). In both cases, the external cavity Raman laser architecture, in which the Raman laser is pumped by a beam generated separately, was the favored approach as it is most applicable to standard pulsed pump laser such as commercially available Nd or Yb laser systems. The initial proposal had planned to investigate the more restrictive intracavity architecture[1] as a contingency in the case that the external cavity conversion was unsuccessful; however, the latter approach proved to work well and this contingency was not needed.

Along with these main streams, work was carried out to characterize the quality and measure pertinent optical properties of the as-supplied diamond material. Modeling of the Raman lasers was also performed to underpin the experiments and provide a tool for predicting performance when increasing output power beyond the scope of this preliminary study. This parallel work is summarized in the Results and Discussion.

1) Power scaling of pulsed DRLs

The basic optical arrangement for the pulsed external cavity Raman lasers is shown in the figure below. The pump laser was based on a commercial side-diode-pumped neodymium vanadate gain modules (Northrop Grumman RBA20-1C2-FR1-1013) and Q-switched using an acousto-optic modulator to generate pulses approximately 20 ns in duration at 30-40 kHz repetition rate. The average output power was up to 50 W. The maximum peak power was approximately 50 kW.

[1] The intracavity architecture takes advantage of the resonantly enhanced fundamental field to lower the Raman threshold and to enable low threshold CW/quasi-CW operation.

The collimated pump beam was focused into the diamond crystal so that the confocal parameter of the pump field closely matched that of the diamond length. The diamond was up to 9.5-mm long, and made of low-nitrogen content, ultra-low birefringence, Type IIa single crystal diamond grown by chemical vapor deposition and supplied by Element 6 (UK). Anti-reflection coated and Brewster cut crystals were investigated.

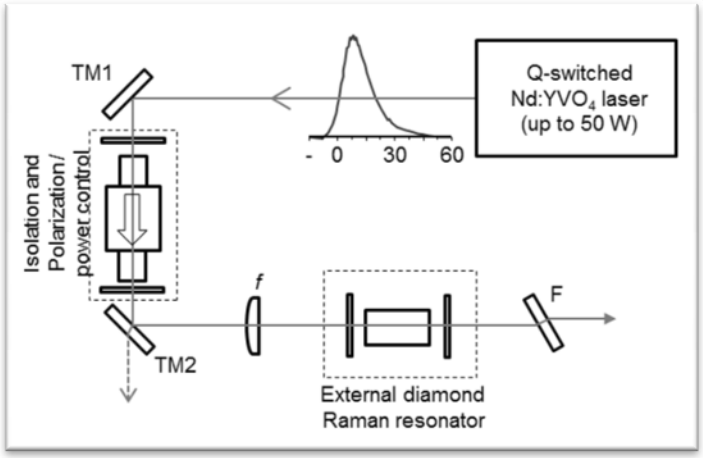

The output power, conversion efficiency and beam properties of the DRL were investigated as functions of the input beam properties and Raman cavity mirrors. The experiments have been detailed in Refs [4,15,17] and the results summarized in [11,12,19].

2) Power scaling of CWDRLs

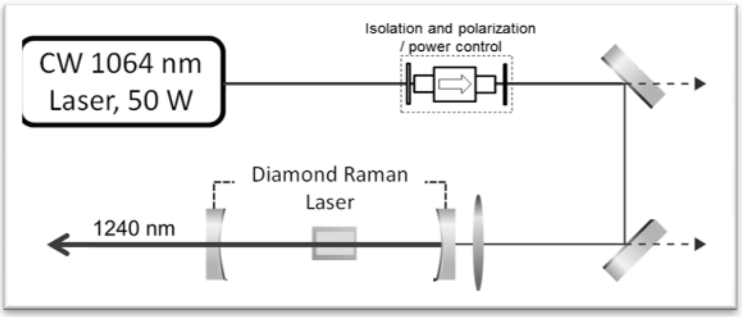

The CW experiments involve the same basic approach but with careful attention paid to cavity losses and to the waist sizes of the pump and Stokes beam in the diamond crystal. Much smaller spot-sizes in the Raman crystal to are used to enable efficient conversion at the typically much lower peak powers of CW operation. The Raman resonator is nearly concentric to provide a small resonated Stokes mode in the Raman crystal. The resonator output coupling is typically less than 1% and the diamond crystals are selected for low absorption loss and low birefringence. The experiments have been detailed in [1,7,9,10] and summarized in [3,6,11, 12,19].

Results and Discussion:

Experimental and/or theoretical research advances or findings and their significance to the field and what work may be performed in the future as a follow on project.

1) Pulsed

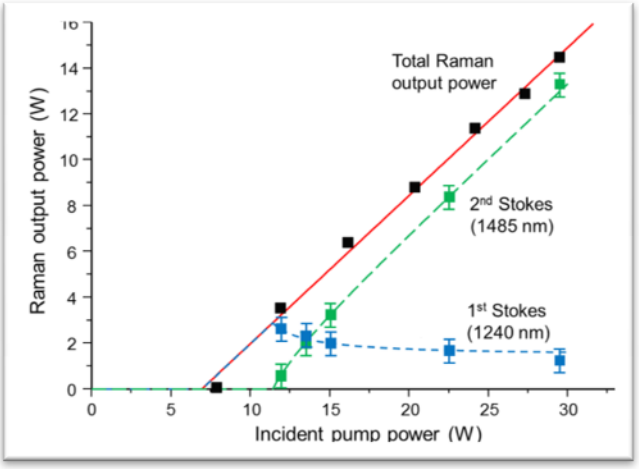

We find that the efficiencies routinely seen at the 1 W output power level are sustainable at powers up to at least 15 W of Raman output power. The system investigated in most detail consisted of a 9.5-mm-long anti-reflection coated diamond slab placed in 2.5-cm long external-cavity Raman resonator and pumped by a 35 W Q-switched Nd:YVO_4 laser generating 22 ns pulses at a 36.5 kHz pulse repetition frequency (preliminary aspects of this work have been reported in [4] attached). The Raman laser mirror set enabled combined first (1240 nm) and second Stokes (1485 nm) output with powers up to 14.5 W at a conversion efficiency of 48.5% (the incident power was 30 W). At maximum power, 13 W was generated at 1485 nm in the eye-safe spectral region.

The total output power is comparable to recent reports in barium nitrate (17 W, Chulkov *et al* 2012) and diamond (combined two-beam output of 24.5 W, Feve *et al* 2011), but with much higher efficiency and using a much simpler overall system[2]. The quantum conversion efficiency is 2.1 times the 17 W barium nitrate and 4.5 times the 24.5 W diamond lasers. The higher efficiency, and the use of a simple and compact high power pump laser compared to these previous studies, is of fundamental importance for applications. Indeed the large fraction of output at 1485 nm, along with the high pulse repetition rate (36.5 kHz) is expected to be of interest for applications of current importance such as rapid scanning remote detection and environmental sensing. The eye-safe power (13 W) is similar to the highest power achieved using high pulse rate the optical parametric oscillators (13.6 W, Dong *et al* 2009), and in-band pumped Er:YAG lasers (9.5 W, Setzler *et al* 2005) which comprise the most prominent 1.5 μm eye-safe laser technologies (see Table below). No optical damage or deleterious thermal effects were observed. The power characteristics agree well with simple rate equation modeling without the need for including thermal effects. We concluded that further increases in power and efficiency are likely to be achieved without the use of thermal lens or birefringence compensation.

Technology	Average Power (W)	PRF	Efficiency	Reference
DIAMOND	**13**	**36 kHz**	**43%**	**This work**
OPO	**13.6**	18 kHz	5.7%*	Dong et al, Opt Commun, 2009
Resonantly pumped Er:YAG	**9.5**	10 kHz	49%	Setzler., IEEE J Sel Top 2005
Non-diamond Raman lasers	**5.2**	20 kHz	20%*	Chen et al., Appl Phys B 2012

*Optical diode-to-output

By using an upgraded 50 W pump laser we have recently observed output powers at 16.1 W at a single Stokes order at 40% conversion efficiency. Our future pulsed investigations will be aimed towards increasing first Stokes and eye-safe laser output power by optimizing the output coupling and by using higher power pumps. Based on literature values for key diamond's thermo-optical properties, which have been summarized by the Principal Investigator in [18], the thermal limiting factors of thermal lensing, thermally-induced stress birefringence and stress fracture, will not come into play until the kilowatt level.

Optical damage to the diamond facets, which was found to limit power in the work of Feve *et al*, is an important consideration when power scaling. We observed damage free operation routinely for incident Q-switched pulse intensities of approximately 300 $MW.cm^{-2}$ and similar circulating intracavity first Stokes intensity. For a second Stokes laser, damage was observed to the anti-reflection coatings when using an output coupler of relatively high reflectivity (R = 60% at the second Stokes) and with estimated cumulative (pump plus Stokes) intensities of approximately 1 $GW.cm^{-2}$.

A further important aspect of this work concerns brightness conversion. We have studied beam quality and efficiency for strongly aberrated pumps, the details of which we will disclose in the near future.

Major conclusions:

1) Pulsed DRLs of maximum power up to 16.1 W have been demonstrated, a 13-times increase over the highest power reported at project start.
2) Conversion efficiencies 40-50% were obtained at this power level (cf., the record for a crystal Raman laser is 64%).
3) Second-Stokes conversion of 1.06 μm pumps to 1.5 μm was demonstrated. The system approach is a promising competing technology for high power (multi-kilohertz) eye-safe lasers.
4) Lack of optical damage and deleterious thermal effects portends good prospects for achieving much higher output by using higher power pumps. Thermal effects in the diamond are expected to become significant at kilowatt power levels.

[2]In the work of Chulkov *et al*, a 60 W Q-switched-burst flashlamp-pumped system was used as the pump source and substantial efforts were put into compensation of the induced Raman lens. For Feve *et al*, the pump source comprised of a cryogenic Yb:YAG laser of average power more than 180 W.

2) <u>Continuous wave</u>

CW conversion has been demonstrated at output powers up to 16 W. An anti-reflection coated slab (9-mm long) was placed in a confocal high-finesse resonator to create an intense Stokes waist within the crystal. For an output coupling of approximately 0.4%, the laser threshold was 10 W of incident power and a maximum output power of 16 W was obtained for 40 W of input power (40% conversion efficiency). This result represents the first external cavity crystal Raman laser pumped using a CW Nd laser at 1064 nm. The output power is more than three times the highest for a CW crystalline Raman laser, that being for a 5.1 W intracavity diamond Raman laser at 1240 nm (Savitski *et al* 2012).

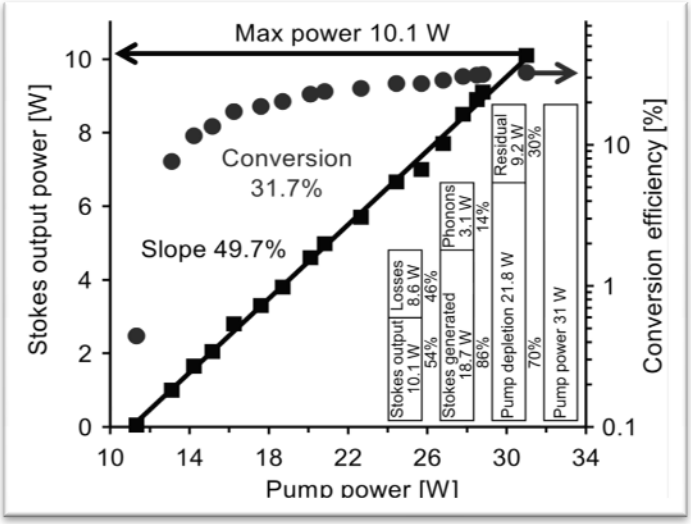

A detailed description and characterization of a 10 W device has been reported in [1]. The output power increased linearly with input power with slope efficiency 50% as shown inset. As in the pulsed converter, no thermal effects were observed suggesting good prospects for maintaining the slope efficiency with more powerful pumps. This is consistent with theoretical predictions. Clean-up of the pump beam was observed for experiments involving a pump with beam quality factor M^2=1.7. The external cavity approach has important benefits for operation at elevated powers. Placement of the Raman crystal at the midpoint of a concentric resonator mitigates the effects of any thermally induced refractive index gradients. Furthermore, it is more straightforward to decouple the thermal lens effects in the pump laser from the Raman laser compared to intracavity designs.

The slope and overall conversion efficiency (50% and 32% respectively) are lower than we typically observed for pulsed systems (65-85% and 40-50%). The configuration was convenient for investigating system losses since the experiment allowed good access to the unconverted pump laser beam. From the pump depletion, representing the difference between pump and unconverted pump upon alignment of the Raman laser cavity, we deduced the total power coupled into the Stokes and phonon fields. The results are summarized in the inset figure above for operation at maximum power. It was concluded that significant power (approximately 8 W) is lost in the bulk diamond due to absorption and/or scatter. Thus in contrast to the pulsed diamond Raman lasers described above, improved crystal quality is expected to markedly increase the conversion efficiency and output powers. Using the known output coupler transmission (0.4±0.1%) and Stokes power circulating in the Raman cavity, the combined absorption and scatter coefficient of the diamond was deduced to be approximately 0.17±0.05%/cm at 1240 nm, which is close to the absorption coefficient value (approximately 0.1%/cm at 1064 nm) for the diamond supplier's low nitrogen (20 ppb) material. Lower loss (i.e., lower nitrogen) diamond is predicted to enable up to 18 W output power at 60% conversion efficiency.

Characterization of diamond birefringence in the beam direction is found to vary significantly within and across samples. Selection of low birefringence crystals may be an important factor affecting threshold and efficiency, and we plan to quantitatively investigate this aspect in the near future.

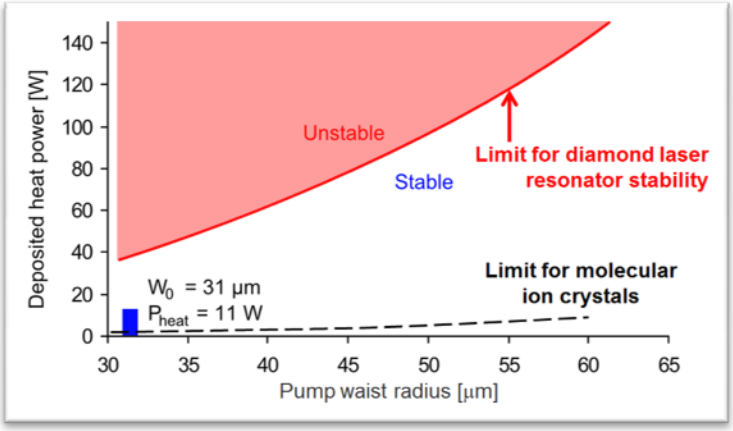

Our calculations suggest that the thermal lens strength will be the major consideration over birefringence, end face curvature and stress fracture. On this assumption, we have calculated

resonator stability as a function of heat deposited in the crystal. For the above specific arrangement with 11.9 W of power deposited in the Stokes beam waist of 31 μm, and we calculate that we are about 3-4 times below the stability limit. Considering also the freedom to reduce the lens strength by increasing the spot-size in the diamond[3], we deduce that output powers of up to several hundred watts are possible without major changes in basic design. In contrast, the power limits for the much thermally less-amenable molecular ion crystalline Raman lasers is two-orders of magnitude lower.

We believe these advances in CW beam conversion are a significant step towards high power CW lasers that can address wavelength specific applications near 1.2 μm and 1.5 μm, and at their harmonics by use of intra- and/or extra-cavity nonlinear frequency generation. The latter is an important advantage over fiber Raman laser technologies. The scheme has the practical advantage of building on very mature high power CW Nd and Yb laser technologies, and potentially other sources of high power CW output such as chemical lasers and alkali vapor lasers. The concept is applicable to mature and powerful 532 nm lasers currently available (in which case the threshold will reduce due to a Raman gain coefficient at the shorter wavelength), in order to generate red-yellow output in the ultraviolet by further nonlinear ($\chi^{(2)}$) frequency generation. The concepts are expected to have commercial value and hence we have taken steps to protect the relevant IP. The only CW pumped external cavity crystal Raman laser reported previously as far as we are aware was for a 6.8 cm-long barium nitrate crystal and using a gas pump laser in the visible (Ar^+; 514 nm) (Grabtchikov *et al* 2005) where the gain is high (approximately 50 cm/GW). For this device the efficiency was low (0.16 W for 5.5 W of pump power), and even at this power level thermal lensing effects in the barium nitrate were noted. Low gain materials having relatively low thermal conductivity (i.e., molecular ion Raman crystals) therefore have the critical problem that the output is restricted to powers not much higher than the laser threshold. Diamond's combined high gain and thermal conductivity presents an opportunity to investigate CW operation using near-infrared laser pumps and at much higher output powers.

Major conclusions:

1) CW external cavity DRLs of maximum power up to 16 W have been demonstrated at 40% conversion efficiency.
2) Beam clean-up from a pump of M^2=1.7 to an M^2=1.1 output beam has been demonstrated at the 10W level.
3) Crystal quality is critical in this application and large (approximately two-fold) increases in conversion efficiency are possible if lower loss diamond becomes available.
4) Lack of optical damage and deleterious thermal effects portends good prospects for achieving up to several hundred watts by using higher power pumps without major design changes.
5) The system is amenable for high power visible and ultraviolet generation via intracavity and/or extracavity $\chi^{(2)}$ nonlinear frequency generation.

Other outcomes

UV surface etching

As an unexpected outcome of our early investigations into laser damage of diamond crystal facets, we observed UV-induced slow etching of diamond surfaces at a rate that increased with the square of the incident fluence up to the ablation threshold. Ablation threshold is taken here to mean the minimum fluence to produce the irregular shaped pit that is characteristic of conventional diamond ablation in the nanosecond regime. For example, for 266 nm pulses of fluence corresponding to 60% of the ablation threshold, pits 400 nm deep were formed after of 30 s exposure at 7 kHz (2.2×10^5 pulses; corresponding to an etch rate of 2 pm/pulse). For lower fluences, the time required to achieve the same depth was much longer in inverse proportion to the square of the intensity. In each case, the average number of atoms removed per pulse is less than an atomic layer. X-ray surface studies have shown that the etched surfaces were oxygen terminated and free of graphite. Moreover, the results to date suggest the etch rate is proportional to the two-photon absorption rate largely irrespective of the surface facet direction, pulse duration in the range 0.02 to 100 ns, and pulse repetition rate. This work has been reported in detail in [2] and was highlighted in *Nature News*[4].

[3] Lens strength scales with the inverse square of the beam size for a given power deposited.

[4] http://www.nature.com/news/2011/110715/full/news.2011.421.html

The details of the UV absorption in the surface layers and subsequent ejection kinetics are not well understood. A separate group had previously seen signs of this effect (Kononenko *et al* 2007) and reported that the presence of oxygen is required for etching. An improved understanding of the mechanism is needed to determine how the etching can be prevented or exploited. It is not yet known whether 3-photon or higher-order multiphoton effects lead to etching and at what maximum wavelength the effect becomes negligible. The etching, which can be performed in air that and is well suited for rapid prototyping of direct-write structures, is also of interest as a novel method for machining of smooth high resolution surface structures in diamond such as laser waveguides.

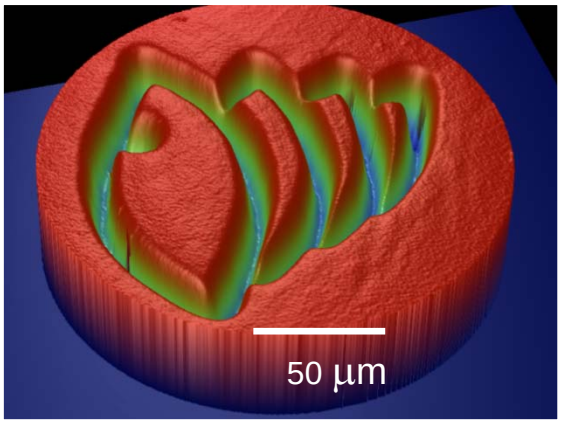

The inset shows, for example, a profile of our University logo of dimensions approximately 100 μm by 100 μm etched into the {100} face of a single crystal diamond. The square-dependence on the intensity is reproduced spatially, so that features can be written smaller than the diffraction-limited spot-size of the writing beam. We aim to investigate the method further to determine whether the etching is able to solve current challenges in the production of long low-loss waveguides.

Overall assessment

Diamond Raman laser technology is highly promising for high power beam conversion and further advances in performance are expected as our research efforts continue. Increases in power and wavelength range are expected in the short term with the currently available material. Parallel advances by crystal growers will also fuel progress, particularly for CW converters in which losses are relatively much more important. With major breakthroughs in the growth of quality large single crystals occurring only in the last decade, it can still be considered early days for synthesis. Reduced absorption and scatter, larger sizes and lower production costs, are currently some directions of development that will assist Raman laser development. Reproducibility and lower cost are also directions that will benefit research and crucial for future transfer of the technology into the commercial arena. Currently CVD growth is perceived to be the most promising method due to its unrivalled level of control on absorbers and residual stress-birefringence. Studies on other sources of material are few as far as we are aware, however, there may be scope for other types of material (e.g., HPHT or polycrystalline material) at least in some configurations where birefringence or scatter loss are not so critical. Longer crystals than the up-to-1 cm-lengths currently investigated may also provide advantages for increasing performance range. Doping of diamond with laser ions represents a highly attractive avenue of development following the success of Nd doped Raman crystals in simplifying intracavity Raman laser design ("self-Raman lasers"). However, the present challenges involved in incorporating a sufficient density of lasant ions into the closely packed diamond lattice are large and a major advance is required before this possibility can be exploited. Diamond waveguides are also an area of current development by us and others that will assist device design via the well-known benefits afforded by beam confinement for enhancing nonlinearity and mitigating thermal effects. Such developments in diamond material engineering create exciting prospects for the field of diamond lasers.

Future development of diamond lasers will be driven by the ever increasing demand for laser devices of enhanced performance range. Our future work is aimed at demonstrating a class of devices for wavelength conversion at the power level usually the domain of fiber or disk lasers and offering a greater range of wavelengths and intrinsically narrower output bandwidths compared to fibers. There are potentially a large range of applications demanding wavelength conversion that may benefit from the high power handling capability offered by diamond.

List of Publications and Significant Collaborations that resulted from the AOARD supported project:

a) papers published in peer-reviewed journals,

[1] Kitzler, O., McKay, A. & Mildren, R.P., 2012. "Continuous-wave wavelength conversion for high-power

applications using an external cavity diamond Raman laser," *Optics Letters*, 37(14), pp.2790–2.

[2] Mildren, R.P., Downes, J E, Brown, J D, Johnston, B F, Granados, E, Spence, D J, Lehmann, A Weston, L, Bramble, A., 2011. "Characteristics of 2-photon ultraviolet laser etching of diamond," *Optical Materials Express*, 1(4), pp.576–585.

b) papers published in peer-reviewed conference proceedings,

[3] Mildren, R.P., 2012. "Recent progress in diamond Raman lasers," *Mater. Res. Soc. Symp. Proc.*, 1395, pp.1–12. **Invited Plenary Session**

c) papers published in non-peer-reviewed journals and conference proceedings,

[4] A. McKay, O. Kitzler, H. Liu, D. Fell, and R.P. Mildren."High average power (11 W) eye-safe diamond Raman laser."*Photonics Asia*, *Conference on High Power Lasers and Applications 8551* (International Society for Optics and Photonics) pp. 85510U-85510U, (2012).

d) conference presentations without papers,

[5] O. Kitzler, A. Sabella, A. McKay and R.P. Mildren, "Characterization of optical quality single crystal diamond for Raman laser applications," XX INTERNATIONAL MATERIALS RESEARCH CONGRESS, 14 - 19 August, Cancún, Mexico, Paper S17-P05 (2011) Poster Paper

[6] R.P. Mildren, "Performance extension of Raman lasers using synthetic diamond," CLEO Pacrim (Sydney) Aug 28-Sep1 Paper 3230-CT-1 (2011) **Invited Paper**

[7] O. Kitzler, A. McKay and R.P. Mildren, "CW diamond laser architecture for high power Raman beam conversion," IQEC/CLEO Pacific Rim (Sydney) Aug 28-Sep1 (2011) **Postdeadline paper**

[8] O. Kitzler, A. Sabella, B.F. Johnston, A. McKay and R.P. Mildren, "Design and characterization of optical quality synthetic diamond for Raman laser applications," IQEC/CLEO Pacific Rim (Sydney) Aug 28-Sep1 Paper 4700-PO-20 (2011)

[9] O. Kitzler, A. McKay and R.P. Mildren, "High average power diamond Raman beam conversion," 2012 MMI-Harvard Diamond Photonics Symposium, (Melb, 17-20 Jan), P8, (2012).

[10] O. Kitzler, A. McKay and R.P. Mildren, "High power CW diamond Raman laser: Analysis of efficiency and parasitic loss," Conference on Lasers and Electro-Optics (6 - 11 May 2012 : San Jose, CA) paper CTh1B.7 (2012).

[11] R.P. Mildren, O. Kitzler, A. M. McKay and H. Liu, "High-power Beam Conversion Using Synthetic-diamond Raman Lasers" High Power Laser and Applications (HPLSA), Istanbul, Paper S11-8 (2012)

[12] R.P. Mildren, O. Kitzler, A. McKay, H. Liu, "Is diamond a good material for wavelength conversion at high power?," Photonics Asia, High-Power Lasers and Applications VI, Conference 8551, 5 - 7 November, Paper 8551-20, (2012)

[13] R.P. Mildren, A. Lehmann, C. Baldwin and J.E. Downes, "Polarization Dependent Nanostructuring of Diamond Surfaces by Two-Photon Ultraviolet Etching," Australian Institute of Physics Congress, UNSW Dec 9-13 (2012)

[14] A. Sabella, J.A. Piper and R.P. Mildren "Impact of pump polarisation and linewidth on the Raman gain coefficient of diamond", Australian Institute of Physics Congress, UNSW Dec 9-13 (2012)

[15] A. McKay, O. Kitzler, H. Liu, D. Fell and R.P. Mildren, "Efficient High-Power Pulse Diamond Raman Laser

Operating in the Eye-Safe Spectral Region" Australian Institute of Physics Congress, UNSW Dec 9-13 (2012)

[16] O. Kitzler, A. McKay and R.P Mildren, "Continuous Wave, 10 W External Cavity Raman laser: Experiment and Modeling," Australian Institute of Physics Congress, UNSW Dec 9-13 (2012)

e) manuscripts submitted but not yet published, and

[17] A. McKay, H. Liu, O. Kitzler, R.P. Mildren, "Efficient 14.5 W diamond Raman laser at high pulse repetition rate with first (1240 nm) and second (1485 nm)Stokes output," *Laser Physics Letters*, submitted 28th Dec 2012, (2013)

[18] R.P. Mildren, "Intrinsic optical properties of diamond," in *Optical Engineering of Diamond* (Wiley) pp1- 34, (2012) (Expected release date March 2013)

[19] R.P. Mildren, A. Sabella, O. Kitzler, D.J. Spence and A. McKay, "Diamond Raman laser design, performance and prospects," in *Optical Engineering of Diamond* (Wiley) pp239-276,(2012) (Expected release date March 2013)

f) provide a list any interactions with industry or with Air Force Research Laboratory scientists or significant collaborations that resulted from this work.

Some of the outcomes of this project have led to a successful 3-year project in ultrafast Raman lasers, jointly funded by industry partner M-Squared Lasers Ltd (UK) and the Australian Research Council[5]). The scope of this project is heavily concentrated on using diamond for wavelength conversion of laser pumps of pulse duration less than 30 ps at multi-watt powers.

The innovations related to high power CW conversion in an external diamond resonator have also stimulated a number of interactions with companies. Once contract agreements are in place, there is good potential for at least two of these to form formal collaborations.

References

Chulkov et al., 2012. Thermal aberrations and high power frequency conversion in a barium nitrate Raman laser. Applied Physics B, 106(4), pp.867–875.

Chen X.H. et al., 2011. Highly efficient double-ended diffusion-bonded Nd:YVO_4 1525-nm eye-safe Raman laser under direct 880-nm pumping. Applied Physics B, 106(3), pp.653–656.

Dong X.-L. et al., 2009. High-power 1.5 and 3.4 μm intracavity KTA OPO driven by a diode-pumped Q-switched Nd:YAG laser. Optics Communications, 282, pp1668–1670.

Feve J.-P. M. et al., 2011. High average power diamond Raman laser. Optics Express 19(2), pp913–922.

Setzler D. et al., 2005. Resonantly pumped eyesafe erbium lasers. IEEE Journal of Selected Topics in Quantum Electronics. 11(3), 645–657.

[5]Spence, Pask, Mildren, Piper, Malcolm, and McConnell "Versatile ultrafast Raman lasers", ARC Grant LP110200545 (2012-2014)

Attachments:

1) **Publications a), b) and c) listed above.**
2) **DD882: Inventions disclosure form.**
3) **SF425 Financial Report.**

Continuous-wave wavelength conversion for high-power applications using an external cavity diamond Raman laser

Ondrej Kitzler,* Aaron McKay, and Richard P. Mildren

MQ Photonics Research Centre, Macquarie University, NSW 2109, Australia

**Corresponding author: ondrej.kitzler@mq.edu.au*

Received April 23, 2012; revised May 29, 2012; accepted May 30, 2012;
posted May 30, 2012 (Doc. ID 167242); published July 3, 2012

We demonstrate continuous-wave (cw) operation of a diamond Raman laser at 1240 nm in an external cavity configuration. The output power increased linearly with pump power with a 49.7% slope efficiency and reached 10.1 W at the maximum available pump power of 31 W. The combination of resonator design with diamond provides a novel approach to power-scalable cw wavelength and beam conversion. © 2012 Optical Society of America

OCIS codes: 140.3550, 140.3580, 160.4330, 190.5650.

High-power cw generation at wavelengths different from rare-earth ion (Nd, Yb, Er, Ho, Tm) lasers and their harmonics remains a challenge. Instead of using alternative laser media, nonlinear frequency conversion in optical parametric sources (OPOs) and Raman lasers is often used to extend the range of available wavelengths. The main advantages of OPOs are the continuous wavelength tuning and the broad spectral coverage from generally visible to the mid-infrared. However, the average power scaling is limited due to thermal loading of the χ^2 nonlinear crystal arising from parasitic absorption leading to phase-mismatch and damage [1]. Raman lasers, on the other hand, offer a simple approach free from phase matching constraints, which can utilize a class of materials with improved thermal properties.

To date Raman fiber lasers, because of the thermal advantages of a distributed active media, offer the highest cw output power of 150 W with 85% efficiency in the infrared [2]. However, for subsequent harmonic conversion, narrow linewidth output needs to be carefully managed and stimulated Brillouin scattering avoided [3]. Bulk crystalline alternatives benefit from very low spectral broadening, which allows for efficient harmonic generation or frequency mixing. Raman crystals, such as metal nitrates and tungstates, have enabled generation of infrared output powers up to 11 W in pulse mode [4] and 3.4 W continuous wave [5]. In the visible, intracavity self-Raman lasers generating 4.3 W at 586 nm, the second-harmonic of the first Stokes, and 5.3 W at 559 nm, the sum frequency of the pump and the first Stokes, have been demonstrated [6]. However, poor thermal properties of these materials prevent straightforward power scaling in the case of external cavity Raman lasers. In the case of intracavity designs, the simultaneous thermal lensing in the laser media and Raman crystal make the power scaling even more challenging.

Recently, synthetic diamond has shown highly efficient visible [7] and infrared [8,9] Raman conversion. Compared to other Raman crystals, diamond's 2 orders of magnitude higher thermal conductivity and low thermal expansion coefficient mitigates thermal problems, such as induced lensing, birefringence, and stress fracture. Already the highest average output powers for pulsed (24.5 W [10]), and cw intracavity Raman lasers (5.1 W [11]) have been demonstrated using diamond. However, further power scaling of these systems is not straightforward. Suitable pulsed (Q-switched) pumps are not widely available due to the complexity of the high average power systems, whereas cw intracavity lasers are limited due to strong and dynamic thermal effects in the gain medium and the associated challenge of optimizing the intensity in the laser and Raman crystals.

We are interested in further power scaling of cw crystalline Raman lasers and to address demand for high-power cw lasers generating at 1.2–1.5 μm and at their harmonics. Diamond's high Raman gain coefficient and excellent thermal properties allow us to use an external cavity architecture in combination with mature high-power cw laser technology. A cw external resonator Raman laser has been demonstrated previously using barium nitrate as a Raman medium and an Ar-ion pump laser at 514 nm [12]. The high gain of barium nitrate at short pump wavelengths (≈50 cm/GW) and the availability of long crystals enabled a moderate (2 W) threshold to be achieved. The poor thermal properties of the Raman material, however, severely limited the output power to below 200 mW with conversion efficiency of only approximately 5%.

Here we report the first external cavity cw Raman laser operating at 1240 nm pumped by a 1064 nm Nd:YVO_4 laser. Using a low-loss diamond crystal, we achieved a threshold of 11.3 W and a slope efficiency of approximately 50%. As far as we are aware our maximum of 10.1 W represents the highest cw crystalline Raman laser power yet reported. By monitoring the unconverted pump power, we deduce the combined absorption and scatter loss in the diamond crystal sample.

The diamond was a low-nitrogen, ultralow birefringence, type-IIa, grown by chemical vapor deposition (CVD) single-crystal (Element6 Ltd) of dimensions $5 \times 9.5 \times 1.2$ mm^3. The birefringence was between 7×10^{-7} and 3×10^{-6} (measured by the manufacturer using Metripol). Antireflective coatings were applied to both end faces ($R < 1\%$ at 1064 nm, $R < 25\%$ at 1240 nm). The linearly polarized pump beam was incident on the 5×1.2 mm^2 diamond face and propagated along the ⟨110⟩ axis.

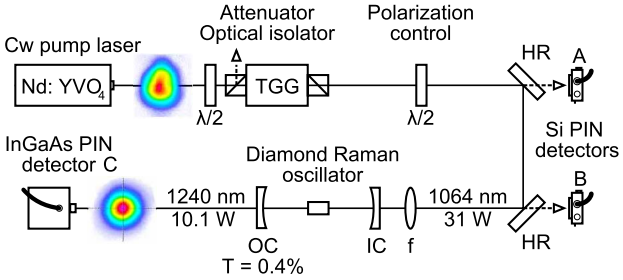

Fig. 1. (Color online) Schema of external cavity diamond Raman laser. Refer to text for explanation of symbols.

The experimental arrangement is shown in Fig. 1. As a pump source we used a cw Nd:YVO_4 laser generating linearly polarized output at 1064 nm. At maximum output the M^2 was approximately 1.7. A half-wave plate and polarizer served as a pump power attenuator. After passing through an optical isolator a half-wave plate was used to align the polarization vector of the pump with the diamond's ⟨111⟩ axis to access the highest gain [8]. In order to reach the threshold of the stimulated Raman scattering, a lens of focal length $f = 50$ mm was used to focus the pump in the diamond. The measured focal spot radius (at $1/e^2$) at the crystal midpoint was 30 μm resulting in an incident intensity of ≈0.8 MW/cm^2 at the threshold of 11.3 W. The pump, residual pump, and Stokes powers were measured by PIN photodiodes A, B, and C calibrated using a power meter.

A 105 mm long quasi-concentric resonator comprised of two concave mirrors with 50 mm radius of curvature was used to mode-match the Raman oscillator and pump waist sizes. The input coupler was highly transmissive at the pump wavelength and highly reflective ($R = 99.99\%$) at the first Stokes wavelength of 1240 nm. The output coupler (OC) was highly reflective at 1064 nm and had 0.4% transmission at the first Stokes wavelength. To prevent generation of the unwanted second Stokes component the mirror reflectivity at 1485 nm was minimized.

Above threshold the Stokes output power increased linearly with input power, as shown in Fig. 2. The maximum output power reached 10.1 W with 31 W of incident pump power. Over the operating range, the residual pump power remained approximately constant at around 10 W. The conversion efficiency at maximum power was

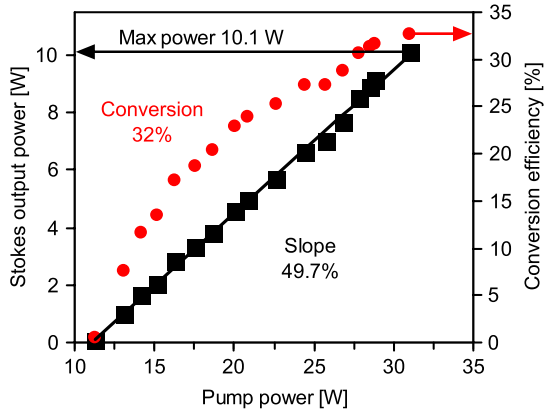

Fig. 2. (Color online) Slope and conversion efficiency of the diamond Raman laser as a function of incident pump power.

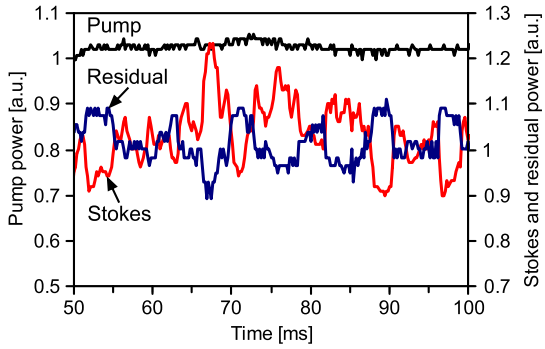

Fig. 3. (Color online) Temporal characteristics of pump, residual pump, and Stokes output radiation.

31.7%. The M^2 parameter improved from 1.7 of the pump to 1.16 of the Stokes (refer to Fig. 1 for far-field images). No optical damage was observed and we expect that much higher output powers can be generated by increasing the pump power.

The Stokes output exhibited substantial amplitude fluctuations when operated near the Raman laser threshold but became more stable at higher pump powers when a significant portion of the pump was depleted. The temporal behavior near maximum power (Fig. 3) shows some fluctuations remaining (about 10% of the average power) correlated with changes in pump depletion. These changes may be caused by mode instabilities observed in the pump laser and mechanical vibrations, which we expect can be reduced by standard techniques.

Simultaneous measurement of the pump power, back-reflected residual pump power, and generated Stokes output power enables the total resonator losses to be deduced. From the pump depletion, representing the change in the residual pump power upon alignment of the Raman laser cavity (from 31 to 9.2 W at maximum pump power), we obtain the power coupled into the Stokes and phonon fields (21.8 W). Of this depleted pump power, 14.2% is lost to the excitation of optical phonons (3.1 W), and the remainder is attributed to the generation of the intracavity Stokes field (18.7 W). Since the measured Stokes output (10.1 W) was 54% of the total Stokes generated, we deduce that the difference (8.6 W) represents the combined parasitic absorption and scatter loss in the diamond.

Well above threshold, the 46% loss fraction of the generated Stokes power was constant as a function of pump power, suggesting linear absorption and scatter loss processes. Using the known output coupler transmission ($T = 0.4 \pm 0.1\%$), we deduce the Stokes power circulating in the Raman cavity and the combined absorption and scatter coefficient in the diamond at 1240 nm. As shown in Fig. 4, the loss coefficient distributed over the crystal length was $0.17 \pm 0.05\%$/cm for the investigated range. We believe this to be an upper bound as there may be some off-axses reflections of the diamond facets. Since the loss coefficient is close to the absorption coefficient value (≈0.1%/cm at 1064 nm) for the diamond supplier's low-nitrogen (20 ppb) material [13], we suspect diamond bulk absorption to be the main loss mechanism. Although slightly higher efficiency may be obtained by optimizing the output coupling, the results of this study show that

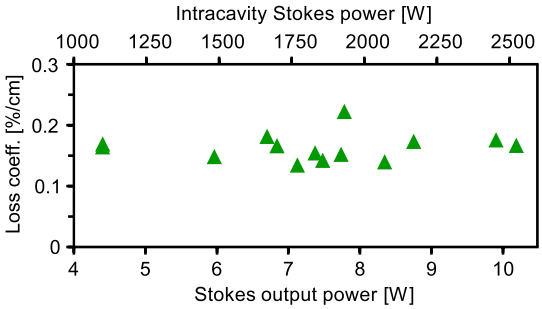

Fig. 4. (Color online) Diamond loss coefficient as a function of Stokes output power. The top axis shows corresponding Stokes intracavity circulating power.

the major limitation for this configuration is diamond loss. Improvements in diamond quality are thus expected to enable slope and conversion efficiencies much closer to the quantum limit (86% for pumping at 1064 nm).

Because of the heating in the crystal arising from inelastic (Stokes) scattering and parasitic absorption (deduced to be approaching 11.7 W in this case), the efficient operation of the device relies on excellent thermal handling properties of the Raman crystal. The superior thermal conductivity and low thermal expansion coefficient of diamond, combined with the concentric resonator design, act to diminish the impact of thermally induced lensing and birefringence as the laser power increases. In addition, the high thermal shock parameter for diamond holds promise for further power scaling without catastrophic damage [14,15].

We have demonstrated efficient conversion of a cw 1064 nm Nd laser to 1240 nm using an external cavity diamond Raman laser with substantial beam quality improvement. The maximum output power of 10.1 W was limited by pump power available, and we expect linear scaling to much higher levels with increased pump power.

The key design attributes of an external Raman resonator and a high gain Raman crystal with excellent thermal properties comprise a power-scalable wavelength conversion approach with intrinsically low spectral broadening (cf., fibers or parametric oscillators). This approach provides a simple add-on device that is applicable to a range of high-power cw laser technologies (including line-narrowed fiber lasers) and with further potential for extending wavelength range via Stokes cascading and subsequent harmonic conversion.

The authors would like to acknowledge the support of an Australian Research Council Future Fellowship (project number FT0990622) and Air Force Research Laboratory (under agreement number AOARD-10-4078).

References

1. Q. Peng, X. Yang, X. Wang, A. Geng, A. Yao, and Z. Xu, Opt. Rev. **12**, 307 (2005).
2. Y. Feng, L. R. Taylor, and D. B. Calia, Opt. Express **17**, 23678 (2009).
3. L. R. Taylor, Y. Feng, and D. B. Calia, Opt. Express **18**, 8540 (2010).
4. V. Lisinetskii, T. Riesbeck, H. Rhee, H. Eichler, and V. Orlovich, Appl. Phys. B **99**, 127 (2010).
5. L. Fan, Y. X. Fan, Y. Q. Li, H. Zhang, Q. Wang, J. Wang, and H. T. Wang, Opt. Lett. **34**, 1687 (2009).
6. A. J. Lee, D. J. Spence, J. A. Piper, and H. M. Pask, Opt. Express **18**, 20013 (2010).
7. R. P. Mildren and A. Sabella, Opt. Lett. **34**, 2811 (2009).
8. A. Sabella, J. A. Piper, and R. P. Mildren, Opt. Lett. **35**, 3874 (2010).
9. A. Sabella, J. A. Piper, and R. P. Mildren, Opt. Express **19**, 23554 (2011).
10. J. P. M. Feve, K. E. Shortoff, M. J. Bohn, and J. K. Brasseur, Opt. Express **19**, 913 (2011).
11. V. G. Savitski, I. Friel, J. E. Hastie, M. D. Dawson, D. Burns, and A. J. Kemp, IEEE J. Quantum Electron. **48**, 328 (2012).
12. A. S. Grabtchikov, V. A. Lisinetskii, V. A. Orlovich, M. Schmitt, R. Maksimenka, and W. Kiefer, Opt. Lett. **29**, 2524 (2004).
13. I. Friel, S. L. Geoghegan, D. J. Twitchen, and G. A. Scarsbrook, Proc. SPIE **7838**, 783819 (2010).
14. J. T. Paci, T. Belytschko, and G. C. Schatz, Chem. Phys. Lett. **414**, 351 (2005).
15. Y. F. Chen, IEEE J. Quantum Electron. **35**, 234 (1999).

Characteristics of 2-photon ultraviolet laser etching of diamond

R. P. Mildren,* J. E. Downes, J. D. Brown, B. F. Johnston, E. Granados, D. J. Spence, A. Lehmann, L. Weston, and A. Bramble

MQ Photonics Research Centre, Macquarie University, Sydney, NSW 2109, Australia
**rich.mildren@mq.edu.au*

Abstract: We report graphite-free laser etching of diamond surfaces using 266 nm laser pulses for a wide range of incident fluences below the threshold for ablation. The etching rate is proportional to the (fluence)^x where $x = 1.88 \pm 0.16$ over the range 10^{-6} - 10^{-2} nm per pulse for incident pulse fluences 1 – 60 J/cm^2. Surface sensitive near edge x-ray fine absorption structure measurements (partial electron yield NEXAFS) reveal that etching does not significantly alter the surface structure from the initial oxygen terminated and graphite-free state. The etching process, which is consistent with a mechanism involving the desorption of carbon species via the decay of 2-photon excited excitons near the surface, appears to have no threshold and is promising for creating a range of high resolution structures.

OCIS codes: (220.1920) Diamond machining; (220.4000) Microstructure fabrication; (220.4610) Optical fabrication; (160.4670) Optical materials; (140.3610) Lasers, ultraviolet.

References and links

1. T. Gaebel, M. Domhan, I. Popa, C. Wittmann, P. Neumann, F. Jelezko, J. R. Rabeau, N. Stavrias, A. D. Greentree, S. Prawer, J. Meijer, J. Twamley, P. R. Hemmer, and J. Wrachtrup, "Room-temperature coherent coupling of single spins in diamond," Nat. Phys. **2**(6), 408–413 (2006).
2. A. Faraon, P. E. Barclay, C. Santori, K.-M. C. Fu, and R. G. Beausoleil, "Resonant enhancement of the zero-phonon emission from a colour centre in a diamond cavity," Nat. Photonics **5**(5), 301–305 (2011).
3. L. Sekaric, J. M. Parpia, H. G. Craighead, T. Feygelson, B. H. Houston, and J. E. Butler, "Nanomechanical resonant structures in nanocrystalline diamond," Appl. Phys. Lett. **81**(23), 4455–4457 (2002).
4. R. P. Mildren, J. E. Butler, and J. R. Rabeau, "CVD-diamond external cavity Raman laser at 573 nm," Opt. Express **16**(23), 18950–18955 (2008).
5. M. Karlsson, K. Hjort, and F. Nikolajeff, "Transfer of continuous-relief diffractive structures into diamond by use of inductively coupled plasma dry etching," Opt. Lett. **26**(22), 1752–1754 (2001).
6. E. Gu, H. W. Choi, C. Liu, C. Griffin, J. M. Girkin, I. M. Watson, M. D. Dawson, G. McConnell, and A. M. Gurney, "Reflection/transmission confocal microscopy characterization of single-crystal diamond microlens arrays," Appl. Phys. Lett. **84**(15), 2754–2756 (2004).
7. M. Tarutani, Y. Takai, and R. Shimizu, "Application of the focused-ion-beam technique for preparing the cross-sectional sample of chemical vapor deposition diamond thin film for high-resolution transmission electron microscope observation," Jpn. J. Appl. Phys. **31**(Part 2, No. 9A), L1305–L1308 (1992).
8. S. Castelletto, J. P. Harrison, L. Marseglia, A. C. Stanley-Clarke, B. C. Gibson, B. A. Fairchild, J. P. Hadden, Y.-L. D. Ho, M. P. Hiscocks, K. Ganesan, S. T. Huntington, F. Ladouceur, A. D. Greentree, S. Prawer, J. L. O'Brien, and J. G. Rarity, "Diamond-based structures to collect and guide light," N. J. Phys. **13**(2), 025020 (2011).
9. W. J. Zhang, Y. Wu, W. K. Wong, X. M. Meng, C. Y. Chan, I. Bello, Y. Lifshitz, and S. T. Lee, "Structuring nanodiamond cone arrays for improved field emission," Appl. Phys. Lett. **83**(16), 3365–3367 (2003).
10. P. Olivero, S. Rubanov, P. Reichart, B. C. Gibson, S. T. Huntington, J. R. Rabeau, A. D. Greentree, J. Salzman, D. Moore, D. N. Jamieson, and S. Prawer, "Ion-beam-assisted lift-off technique for three-dimensional micromachining of freestanding single-crystal diamond," Adv. Mater. (Deerfield Beach Fla.) **17**(20), 2427–2430 (2005).
11. M. Rothschild, C. Arnone, and D. J. Ehrlich, "Excimer-laser etching of diamond and hard carbon films by direct writing and optical projection," J. Vac. Sci. Technol. **4**(1), 310–314 (1986).
12. A. Piqué and D. B. Chrisey, *Direct-Write Technologies for Rapid Prototyping Applications: Sensor, Electronics, and Integrated Power Devices* (Academic Press, 2002), p. 440.
13. D. J. Ehrlich and J. Y. Tsao, "A review of laser–microchemical processing," J. Vac. Sci. Technol. B **1**(4), 969–984 (1983).
14. I. P. Sytov, "Estimation of the capabilities of maskless micropatterning by laser-induced chemical etching," Appl. Phys., A Mater. Sci. Process. **61**(1), 75–80 (1995).

#149550 - $15.00 USD Received 21 Jun 2011; revised 4 Jul 2011; accepted 4 Jul 2011; published 12 Jul 2011

15. V. V. Kononenko, M. S. Komlenok, S. M. Pimenov, and V. I. Konov, "Photoinduced laser etching of a diamond surface," Quantum Electron. **37**(11), 1043–1046 (2007).
16. E. Granados, D. J. Spence, and R. P. Mildren, "Deep ultraviolet diamond Raman laser," Opt. Express **19**(11), 10857–10863 (2011).
17. S. Preuss and M. Stuke, "Subpicosecond ultraviolet laser ablation of diamond: nonlinear properties at 248 nm and time-resolved characterization of ablation dynamics," Appl. Phys. Lett. **67**(3), 338–340 (1995).
18. A. Stacey, B. Cowie, J. Orwa, S. Prawer, and A. Hoffman, "Diamond C 1s core-level excitons: surface sensitivity," Phys. Rev. B **82**(12), 125427 (2010).
19. V. V. Kononenko, T. V. Kononenko, S. M. Pimenov, V. I. Konov, P. Fischer, V. Romano, H. P. Weber, A. V. Khomich, R. A. Khmelnitskiy, and V. N. Strekalov, "Laser-induced structure transformations of diamonds," Proc. SPIE **5121**, 259–270 (2003).
20. A. Harasaki, J. Schmit, and J. C. Wyant, "Improved vertical-scanning interferometry," Appl. Opt. **39**(13), 2107–2115 (2000).
21. Y. Muramatsu, K. Shimomura, T. Katayama, and E. M. Gullikson, "Total electron yield soft x-ray absorption spectroscopy in the CK region of the mixtures of graphitic carbons and diamond for quantitative analysis of the sp2/sp3-hybridized carbon ratio," Jpn. J. Appl. Phys. **48**(6), 066514 (2009).
22. J. C. Zheng, X. N. Xie, A. T. S. Wee, and K. P. Loh, "Oxygen-induced surface state on diamond (100)," Diamond Related Materials **10**(3-7), 500–505 (2001).
23. H. Jeschke and M. Garcia, "Theoretical description of the ultrafast ablation of diamond and graphite: dependence of thresholds on pulse duration," Appl. Surf. Sci. **197–198**, 107–113 (2002).
24. B. Luther-Davies, A. V. Rode, N. R. Madsen, and E. Gamaly, "Picosecond high-repetition-rate pulsed laser ablation of dielectrics: the effect of energy accumulation between pulses," Opt. Eng. **44**(5), 051102 (2005).
25. M. J. A. de Dood, A. Polman, T. Zijlstra, and E. W. J. M. van der Drift, "Amorphous silicon waveguides for microphotonics," J. Appl. Phys. **92**(2), 649–653 (2002).
26. J. Smedley, C. Jaye, J. Bohon, T. Rao, and D. A. Fischer, "Laser patterning of diamond. Part II. Surface nondiamond carbon formation and its removal," J. Appl. Phys. **105**(12), 123108 (2009).
27. J. Smedley, J. Bohon, Q. Wu, and T. Rao, "Laser patterning of diamond. Part I. Characterization of surface morphology," J. Appl. Phys. **105**(12), 123107 (2009).
28. S. K. Sudheer, V. P. M. Pillai, and V. U. Nayar, "Characterization of laser processing of single-crystal natural diamonds using micro-Raman spectroscopic investigations," J. Raman Spectrosc. **38**(4), 427–435 (2007).
29. D. Ramanathan and P. A. Molian, "Micro- and sub-micromachining of Type IIa single crystal diamond using a Ti:sapphire femtosecond laser," J. Manuf. Sci. Eng. **124**(2), 389–396 (2002).
30. M. Shinoda, R. R. Gattass, and E. Mazur, "Femtosecond laser-induced formation of nanometer-width grooves on synthetic single-crystal diamond surfaces," J. Appl. Phys. **105**(5), 053102 (2009).
31. C. Bandis and B. B. Pate, "Electron emission due to exciton breakup from negative electron affinity diamond," Phys. Rev. Lett. **74**(5), 777–780 (1995).
32. M. Frenklach, D. Huang, R. E. Thomas, R. A. Rudder, and R. J. Markunas, "Activation energy and mechanism of CO desorption from (100) diamond surface," Appl. Phys. Lett. **63**(22), 3090–3092 (1993).
33. J. Ristein, W. Stein, and L. Ley, "Defect spectroscopy and determination of the electron diffusion length in single crystal diamond by total photoelectron yield spectroscopy," Phys. Rev. Lett. **78**(9), 1803–1806 (1997).
34. J. Cui, J. Ristein, and L. Ley, "Low threshold electron emission from diamond," Phys. Rev. B **60**(23), 16135–16142 (1999).
35. D. Zeisel, S. Nettesheim, B. Dutoit, and R. Zenobi, "Pulsed laser-induced desorption and optical imaging on a nanometer scale with scanning near-field microscopy using chemically etched fiber tips," Appl. Phys. Lett. **68**(18), 2491–2492 (1996).
36. H. Yoshida, Y. Yamashita, M. Kuwabara, and H. Kan, "Demonstration of an ultraviolet 336 nm AlGaN multiple-quantum-well laser diode," Appl. Phys. Lett. **93**(24), 241106 (2008).

1. Introduction

There is currently intense interest in diamond micro- and nano-structured devices for use in applications as diverse as quantum information science [1,2], nano-electromechanical systems [3] and diamond Raman lasers [4]. Diamond is one of the most challenging materials to process due to its extreme mechanical hardness and chemical inertness, and further complicated by crystal planes that behave differently under mechanical and plasma processing. A variety of methods for diamond surface structuring have been investigated including inductively-coupled plasma etching [5,6], ion beam milling [7,8], plasma reactive ion etching [9], ion-implantation with chemical etching [10], and laser ablation [11]. Laser ablation has the convenience of being a direct write process, but there are major challenges in creating high resolution and graphite-free features. An optical etching process that can offer increased resolution without causing graphitization and underlying damage will allow much greater flexibility than currently available.

Laser induced desorption (LID) may be distinguished from laser ablation by lower incident pulse fluences and intensities, and by a mechanism of mass removal that involves

#149550 - $15.00 USD Received 21 Jun 2011; revised 4 Jul 2011; accepted 4 Jul 2011; published 12 Jul 2011

bond breaking and ejection of surface atoms or molecules via the decay of electronically or vibrationally excited quanta rather than via thermo-mechanical or electrostatic forces (e.g [12,13].). LID has been observed in a wide variety of materials with desorption rates dependent on many variables in addition to the photon energy and fluence such as the substrate temperature and the presence of chemical reactants at the surface. Material removal rates are typically less than an atomic layer per pulse and can be achieved without substantial heating of the substrate. As a result, the technique is well suited to a range of surface atomic and molecular diagnostics such as laser mass spectrometry (including biomolecular analysis using matrix assisted laser desorption and ionisation) and surface chemistry studies in addition to micro and nano-structuring applications [14]. For diamond, LID has been observed recently by using pulsed near band-gap laser irradiation [15,16]. Kononenko *et al* [15] showed that diamond was etched in air at rates $0.1\text{-}1\text{x}10^{-3}$ nm/pulse, which is orders of magnitude slower than rates typical of ablation (> 1 nm/pulse [17]), when using sub-ablation threshold laser pulses of wavelength 248 nm. In studies of UV pumped diamond Raman lasers, pits approximately 50 nm deep were etched into the uncoated facets by repeated exposure to 266 nm laser pulses of duration 30 ps, with etch rates as low as tens of carbon atoms per pulse [16].

Improved knowledge on the desorption mechanism is crucial for assessing the flexibility and utility of LID in creating diamond micro- and nano-structures. In etching reports to date [15,16], the rate is a nonlinear function of the incident pulse fluence. Kononenko *et al* [15] also noted that the presence of oxygen at the surface was crucial to the etching process and proposed that the likely mechanism for material ejection was by enhanced oxidation of the surface due to two-photon excitation of electron hole pairs near the surface. The fine control afforded by LID-based etching heralds substantial promise for expanding the range of diamond structures possible using versatile all-optical processes. However, the characteristics of diamond LID are not well known and further investigation is required in order to determine resolution limits of the process and the properties of the etched surface.

In this paper, we report a detailed characterisation of the etch rate and etched surface structure upon exposure to pulsed deep ultraviolet radiation. We show that the etch rate closely follows a square relationship with the incident pulse fluence, as expected for a 2-photon process, and that this relationship holds across the incident beam profile and over a large range of incident fluences up to the ablation threshold. Surface sensitive partial electron yield near edge x-ray absorption fine structure (NEXAFS) spectroscopy shows that etched surface is oxygen terminated and graphite free. We deduce that the process is thresholdless and highly promising for creating a range of smooth structures with spatial resolution at least down to the micron scale.

2. Experimental Description

Single crystal Type IIa (Electronic grade, Element 6) and polycrystalline (Diafilm, Element 6) diamond samples were studied. The surfaces were cleaned using a hot oxidizing acid solution to ensure an oxygen terminated surface. The samples were irradiated using a 266 nm laser (JDSU Q-series Q-201HD 532 nm with custom second-harmonic conversion) of pulse duration 11 ns, pulse repetition rate 7-14 kHz and incident powers up to 300 mW. The linearly-polarized output beam was focused using a 25 mm focal length objective (LMU-5X-UVB, Thorlabs) to a $\omega_0 = 4.8 \pm 0.2$ μm radius spot on the sample surface. Standard definitions for ω_0 and fluence which refer to the radius at the $1/e^2$ value of the maximum with spot area taken as $\pi\omega_0^2/2$ were used. In order to investigate etch rates as a function of fluence for fixed spatial properties of the incident beam, it was important to operate the laser at a fixed output power and attenuate the beam prior to the focusing using a combination of reflective filters with low residual absorption.

The depth, shape and roughness of the etched surface were measured using an interferometric profiler (VEECO, Wyko NT3300). Surface composition and electronic structure were investigated using NEXAFS using the high resolution soft x-ray spectroscopy beamline at the Australian Synchrotron (Melbourne, Australia). The background pressure

#149550 - $15.00 USD Received 21 Jun 2011; revised 4 Jul 2011; accepted 4 Jul 2011; published 12 Jul 2011

during these measurements was 10^{-10} mb. The measurements were performed in partial electron yield mode, to maximise the surface sensitivity of the technique [18].

3. Results

The morphology of laser treated diamond surfaces was investigated as a function of incident fluence both above and below the ablation threshold for [100] Type IIa samples. The threshold is defined here as the minimum laser fluence for ablation damage when using a burst of 60 laser pulses with a duration of approximately 50 ms (corresponding to the shortest exposure time available from the shutter) and corresponds to 37 ± 3 µJ of incident energy or pulse intensities of I_p = 9.2 GW/cm^2 (101 J cm^{-2} in 11 ns). Figures 1(a)–1(c) shows microscope images of the exposed surface for laser intensities 1.1, 0.6 and 0.07 times the threshold. Just above the ablation threshold, pits approximately 10 times the diameter of the incident beam were ablated within the minimum exposure time. The ablated pit typically exhibits cleavage along major crystal planes (eg., [111]) and dross typical of explosive mechanical ejection of large particles. The depth created during the 60 pulse burst corresponds to an approximate ablation rate of 1500 nm/pulse. The ablation rate and morphology is consistent with the strong laser interaction of the beam with the sample via the production of graphite characteristic of nanosecond ablation reported previously (see e.g [19].).

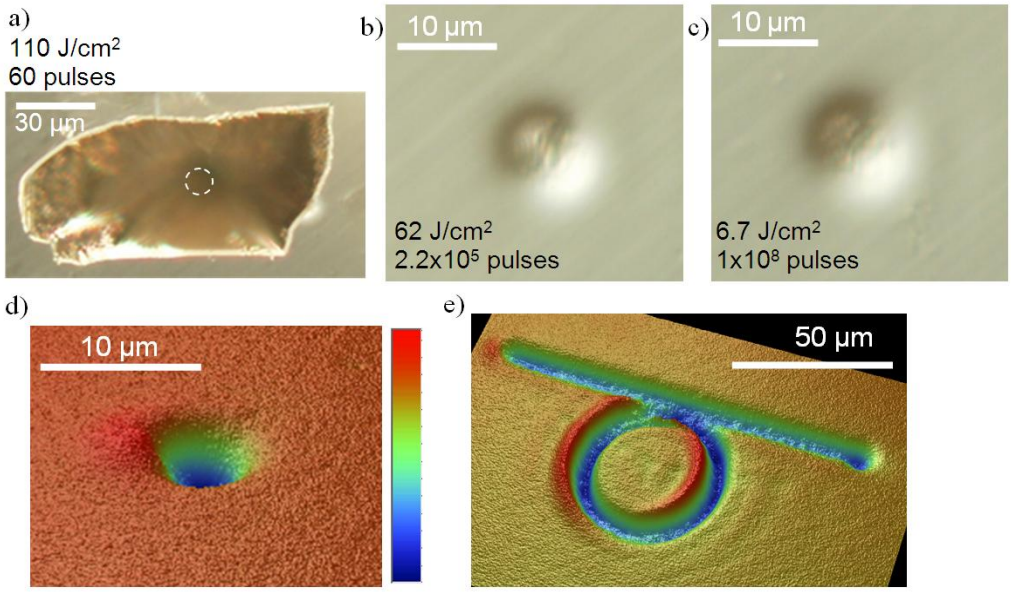

Fig. 1. Microscope images of the diamond surface subsequent to exposure at a) 1.1, b) 0.6 and c) 0.07 times the ablation threshold. The exposure times and depths were 0.05 s, 30 s, 14083 s and 30 µm, 0.60 µm, 0.67 µm respectively, and the pulse rate 7.5 kHz. In a), the beam size is indicated by the dashed circle. For b) and c), the contrast was enhanced using differential interferometric contrast mode. d) 3-D rendered optical interferometric profile image of the pit in b). e) An example of an arbitrary pattern created by the direct write process using a scan speed of 9 µm/s and 120 repetitive scans. Note that in d) and e), the colour bar spans a range of 600 nm and 350 nm respectively, and the raised section on one side of ablated regions where there is discontinuity in the gradient is a known artifact of the measurement system [20].

Below the ablation threshold, the material removal rate is orders of magnitude slower and pits are only observable using a microscope when using much longer exposure times (> 5s). Etched pits of depth less than 1 micron and aspect ratio less than 0.15 were investigated in order to avoid side-wall effects on the etch rate and shape. In this regime, the depth is proportional to the number of cumulative pulses as shown in Fig. 2 for the case of the incident

#149550 - $15.00 USD Received 21 Jun 2011; revised 4 Jul 2011; accepted 4 Jul 2011; published 12 Jul 2011

fluence 34 J cm^{-2} and yielding an average etch rate of 6.4x10^{-4} nm/pulse. Incubation effects on the etch rate during the initial exposure period, if present, are not observable for the typically large number of pulses used (>10^5). The etched-pit morphology is in stark contrast to ablation; the pits are of similar diameter to the incident beam, are smooth and appear on the front and back sides of the sample. All analysis presented herein is on the microstructures of the first surface to avoid complications in the analysis arising from the subsequent defocusing of the transiting beam.

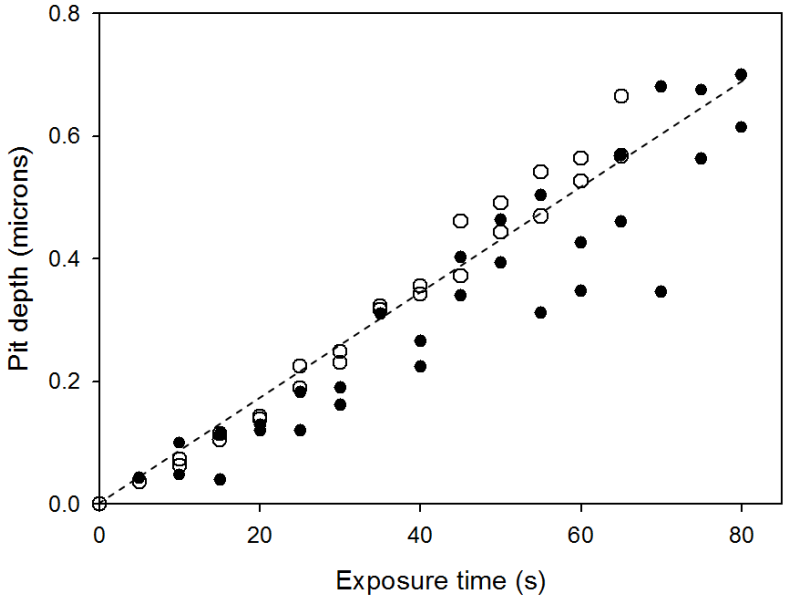

Fig. 2. Etch depth as a function of exposure time. The open circles are for [100] single crystal and the closed circles for polycrystalline material. The dashed line indicates an average etch rate of 6.4x10^{-4} nm/pulse. Conditions: 170 mW at 14 kHz.

Vertical scanning interferometric profile measurements (see for example Fig. 1(d)) reveal that the pits are approximately Gaussian shaped. For pits of Figs. 1(b) and 1(c), the maximum depths are 600 nm and 680 nm respectively and full-width half maxima are 4.3 µm and 5.3 µm. The slightly wider pit of Fig. 1(c), which was created over a period of 2-3 hours, is attributable to drift in the focal spot position that occurs for the system over extended periods. The pit in Fig. 1(b) was etched in a 30 s period and represents the minimum width observed. Figure 3 shows a comparison of the pit etched with incident laser beam profile. The pit width is narrower than the beam and more closely follows the square of the beam profile, i.e., the pit width is approximately equal the beam width divided by √2. Taking into consideration uncertainties in the beam and pit profiles, the pit and beam widths are consistent with an I_p^2 relationship between the etch rate and the incident intensity as discussed in more detail below.

The etch rate as a function of pulse fluence varies nonlinearly with fluence up to the ablation threshold as shown in Fig. 4. Rates were measured for the range 1-60 J cm^{-2} by varying the time period for etching to etch pits of depth in the range (100-800 nm) and using the fact that the etch depth is proportional to the number of incident pulses for all fluences (refer Fig. 2). This procedure ensured that etch rates could be measured accurately over several orders of magnitude whilst maintaining a pit aspect ratio sufficiently small (<15%) to avoid side-wall effects during the etching process and depth measurement procedure. Just below the ablation threshold (60 J cm^{-2}), the etch rate was 2.5 × 10^{-3} nm/pulse. As the fluence was decreased, the etch rate decreased with approximately the square of the incident power. A least squares regression to the data yields a dependence of I_p^x where x = 1.88 ± 0.16 with uncertainty taken as twice the variance. The power factor is consistent with the I_p^2 relationship

#149550 - $15.00 USD Received 21 Jun 2011; revised 4 Jul 2011; accepted 4 Jul 2011; published 12 Jul 2011

expected for a two-photon process underpinning the desorption rate. At low fluences (1.1 J cm^{-2}), the etch rate is less than 10^{-6} nm/pulse which corresponds to approximately 27 000 atoms/pulse over the area of the beam or approximately 0.001% of the exposed surface atoms.

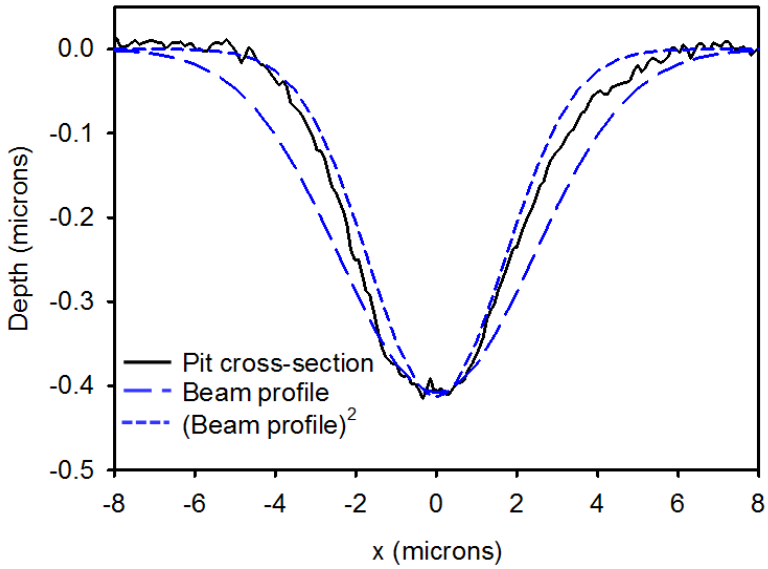

Fig. 3. Comparison of the etch profile with an inverted Gaussian profile of width equal to the measured beam waist. Conditions: 14 kHz pulse rate in air.

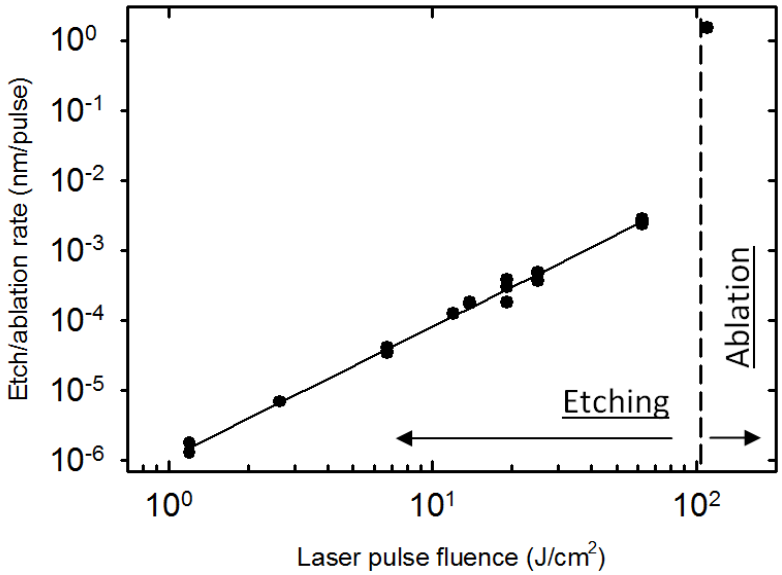

Fig. 4. Etch rate as a function of laser fluence. The data point shown for the fluence above the ablation threshold corresponds to the average ablation rate per pulse for 60 pulses of fluence 110 J/cm^2. Pulse rate 7.5 kHz.

Analysis of the etched surface smoothness and chemical structure was undertaken using the optical interferometric profile and NEXAFS spectroscopy measurements. For both these procedures it was important to create a larger etched region, which was achieved by placing the sample on a computer controlled compound stage and slowly translating the sample (at rates typically < 10 μm s^{-1}). In this manner arbitrary shaped etch patterns could be created as

#149550 - $15.00 USD Received 21 Jun 2011; revised 4 Jul 2011; accepted 4 Jul 2011; published 12 Jul 2011

shown in Fig. 1(e). After etching to 300 nm deep, the rms roughness of the surface increased from 1 nm to 3 nm as measured using the phase shift interference mode of the optical profilometer.

The NEXAFS measurements were undertaken in the range 280-305 eV (C K-edge) in partial electron yield mode with an electron analyzer energy of 165 eV, for which the mean free path of Auger electrons, and thus the surface sensitivity, corresponds to a few (<5) atomic layers. A rectangular area 430 µm x 200 µm wide was etched to match the expected spot size of the synchrotron beam. The etch depth was 50 nm. An ablated 500 µm rectangular grid was placed around the etched area to enable the etched surface to be conveniently located in the NEXAFS spectrometer. The NEXAFS spectrum for the etched surface is presented in Fig. 5 (blue curve). The bulk x-ray absorption edge occurs at 289 eV, with the observation of a strong C 1s core-hole exciton resonance. The pre-edge region contains information on unoccupied surface electronic states within the band gap. Two clear features of differing origin are observed. Feature A is associated with sp^2 hybridized carbon [18,21]. The spectrum for freshly cleaved highly oriented pyrolytic graphite (also included in Fig. 5) clearly shows the peak energy and magnitude corresponding to a graphite surface. The small sp^2 signal appearing in the spectrum of the etched surface is not attributed to generation of etching-induced sp^2 but due to slight overlap of the x-ray beam with the graphite-containing locating grid as confirmed by comparison with the spectrum of the virgin surface containing an ablated grid of twice the density (red curve). Feature B is associated with oxygen termination and in particular the 'top' bonded (ketone) oxygen [22]. The similar areas of B in the etched and un-etched spectra indicate no major change in the level of 'top' bonded oxygen termination between the initial chemically oxidized surface and the laser etched one.

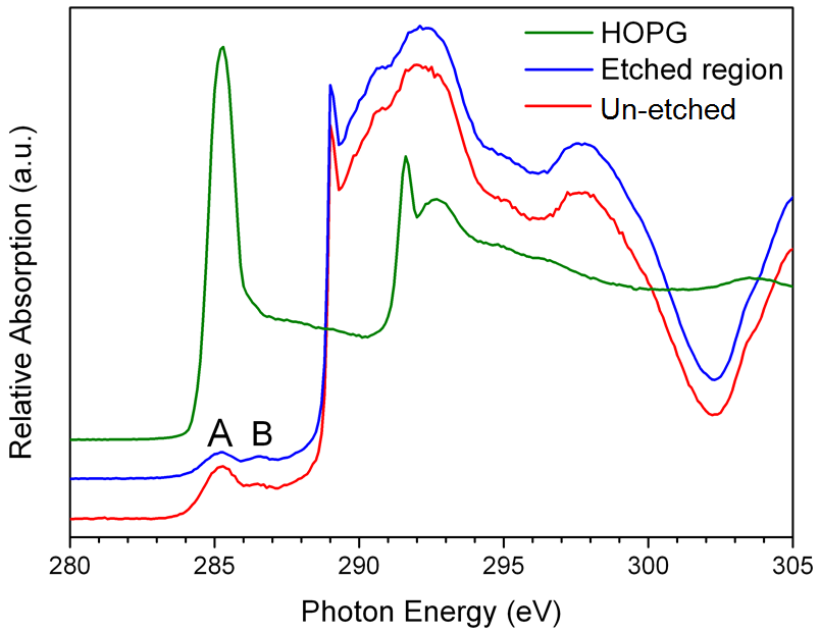

Fig. 5. NEXAFS spectrum for the laser etched surface compared with spectra for high oriented pyrolitic graphite (HOPG) and the un-etched surface. Feature A indicates sp^2 hybridized carbon which appears in the etched and un-etched spectra due to presence of graphite containing locator grids.

3. Discussion

The observed etch rate and surface analysis of the treated surface allow us to make the following conclusions about the etching process:

#149550 - $15.00 USD Received 21 Jun 2011; revised 4 Jul 2011; accepted 4 Jul 2011; published 12 Jul 2011

1. Etching is observed at pulse fluences and peak powers at least two orders of magnitude lower than characteristic fluences for ablation. The etch rate scales with approximately the square of intensity and this relationship is reproduced as a function of position on the surface in accordance with the incident beam profile.

2. The intrapulse etch rate, defined here as the etch depth per pulse divided by the pulse duration FWHM, has a similar dependence on pulse irradiance for ns and ps pulses. When plotted alongside the picosecond measurements of ref [16] (20 ps pulses at 78 MHz repetition rate) and the 248 nm results in ref [15] (15 ns pulses at 100 Hz) as shown in Fig. 6, it is evident that the intrapulse etch rates have a similar dependence on incident intensity suggesting that the rate is largely independent of pulse duration in the range 10^{-10} – 10^{-8} s and pulse repetition rate in the range 10^{2} - 10^{8} Hz. The I_p^2 dependence observed in this study reveals a proportional relationship between the energy absorbed by the two-photon process (proportional to $\beta I_p^2 \Delta t$ where β is the TPA coefficient and Δt is the pulse duration) and the number of ejected atoms. The etch rate for 15 ns pulses at 248 nm at pulse repetition rate <100 Hz [15] also shows similar dependence but at a systematically higher rate. The higher rate may partially result from the higher TPA coefficient for the shorter wavelength (β_{248} = 1.60 cm GW^{-1} and β_{266} = 1.48 cm GW^{-1} [17]), although this is not enough to completely explain the difference. The observed independence with pulse repetition rate from 78 MHz to less than 100 Hz is expected given that multi-pulse effects are unlikely to be significant due to the short relaxation time of free carriers and surface thermal gradients (less than a nanosecond [23,24]) compared to the interpulse period.

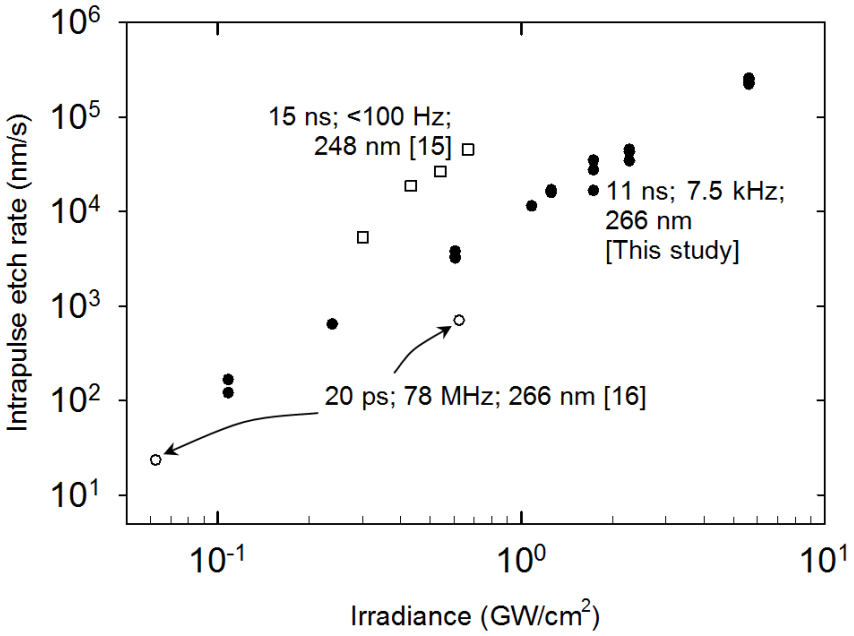

Fig. 6. Comparison of the intrapulse etch rate as a function of pulse irradiance (filled circles) with etching for 20 ps pulses at 266 nm and 78 MHz repetition rate reported in ref [16] (hollow circles) and for 15 ns pulses at 248 nm and pulse rate <100 Hz [15] (hollow squares).

3. The surface roughness increases from 1 nm to 3 nm upon etching to a depth of 300 nm. Low roughness is crucial in many applications, to reduce scattering losses in optical applications for example, and to improve device performance in electronics and MEMS. For waveguides in Si, scattering losses less than the order of the absorption losses are typically obtained for roughness values the order of 5-10 nm (see for

#149550 - $15.00 USD Received 21 Jun 2011; revised 4 Jul 2011; accepted 4 Jul 2011; published 12 Jul 2011

example [25]). Thus 2-photon etching is promising for creating a range of low scatter loss optical surfaces.

4. The etched surface is oxygen terminated and free from graphite. In contrast, graphite formation is intrinsic to laser ablation [11,17,26–28], and ablated features are often characterized by cracking, spalling, crater-halo and debris [28,29]. Although ultrafast machining has enabled reduced formation of graphite [17], and improved resolution [17,30], the absence of graphite in the etched surface observed herein is crucial to enabling linear cumulative etching (as shown in Fig. 2) and an advantage for avoiding post processing (such as ozone, plasma, annealing or chemical treatments).

5. Etching is found to proceed at rates largely independent of the facet direction. We observe etch rates for [100] and polycrystalline surfaces within approximately 20% (as shown in Fig. 2). Etching was also reported [16] for Brewster angled surfaces (63.7 degrees from [110]) at rates similar to the present study when taking into consideration the shorter pulse duration (see Fig. 6). We have also undertaken preliminary etching investigations of polished [110] surfaces which suggest that etching also proceeds at a rate similar to that seen for other surfaces.

These observations reveal that UV etching of diamond in air is a promising and highly versatile method for slow and controlled removal of surface atoms. The most striking observation is the I_p^2 dependence of the etch rate over a large range of pulse durations and pulse rates. Such a well-defined etch rate dependence spanning 3 orders of magnitude, which has not been seen in any other material as far as we are aware, is indicative of a mechanism of particle ejection that is a direct consequence of TPA. TPA by the surface atoms and in the bulk needs to be considered. We discount TPA in the air adjacent the surface due to the small cross-section for TPA in any major air constituents and due to the weak influence on etch rate we observe in the pressure range 1-1000 mb. Kononenko *et al* deduced that thermal processes were too small to account for any observed enhancement of surface oxidation and proposed that surface oxidation was mediated by electron-hole recombination in the diamond bulk [15]. At room temperature, electron hole pairs in diamond form Wannier-Mott excitons with binding energy 80 meV and potential energy just below the indirect band gap [31]. These excitons may diffuse to the surface and give up the stored energy (5.2 eV) to break surface bonds. The exciton energy is sufficient to desorb CO from [100] surfaces, for example, which has an activation energy of desorption of 1.67 eV [32]. If exciton decay at the surface is the dominant cause of desorption, the diffusion length of excitons will be a crucial parameter determining the etching rate and the minimum spatial resolution of etched structures. One would expect that the minimum feature size would be comparable to, or longer than, the diffusion length L_{ex}. Our results suggest that L_{ex} is less than a few microns to account for the observed diameter of the etch pit of less than 5 μm. An upper bound of 5 μm for L_{ex} was deduced on the basis of photo-electron emission yield measurements [33]. However, there seems to be some uncertainty in the value with other reports suggesting values from 200 nm [31] to 200 μm [34]. We note that if L_{ex} < 200 nm, the calculated probability for an exciton created by TPA within L_{ex} of the surface to eject a single carbon atom exceeds unity. If L_{ex} is longer than 5 μm, it may be necessary to consider absorption in the adsorbed oxygen layer to account for the sub-5 μm resolution observed herein.

A notable corollary of the two-photon desorption mechanism at sub-ablation fluences is that etching persists for very low UV fluences, and that even under incoherent illumination diamonds will steadily lose mass. However, the effect under ambient light conditions is rather insignificant. For example, continuous wave Hg lamp illumination at 253 nm for typical irradiances (0.1 W cm^{-2}) would require approximately 10^{10} years to desorb a significant mass (e.g. 1 μg) from a surface a few millimetres square. Under sunlight conditions the etching rate is even slower due to the reduced irradiance (10^{-4} W cm^{-2}; 300-350 nm) and the reduced probability for TPA at longer wavelengths. Of more practical significance, the I_p^2 dependence is of interest for enabling etching using methods other than laser direct-write and sources

#149550 - $15.00 USD Received 21 Jun 2011; revised 4 Jul 2011; accepted 4 Jul 2011; published 12 Jul 2011

other than Q-switched and ultrafast lasers. The field enhancement provided by wavelength scale probe structures (such as those used in scanning near field microscopy) can provide adequate etch rates at small pulse energies (eg., [35]). Projection of patterns using broad area mask imaging and interferometric methods are also interesting avenues for creating high resolution structures. Progress in AlGaN quantum well diode lasers emitting in the deep UV regime (see. e.g [36].) may lead to highly compact sources suitable for etching small areas. Depending on the aforementioned diffusion characteristics of the two-photon excited state, the combination of high resolution scanning methods and pulse fluences corresponding to near single atom removal rates may be an attractive and flexible technique for atomic removal from diamond surface atoms with near single atom precision.

In conclusion, etching of diamond in air is observed at etch rates 10^{-6}-10^{-3} nm/pulse using nanosecond pulses at 266 nm. The oxygen termination of the surface is preserved and free from sp^2 hybridized carbon and graphite. Carbon removal is proportional to TPA of the incident beam and occurs over a large range of fluences up to the ablation threshold. The absence of a threshold indicates substantial promise for enabling a wide range of high resolution structures using diverse techniques such as direct write processing, near-field, masking and interferometric illumination.

Acknowledgments

The authors thank Prof Vitaly Konov for interesting discussions on this subject, Adam Joyce, Carlo Bradac and Törsten Gaebel for their expert assistance in the surface profile analysis methods, and Dr Bruce Cowie for his expert assistance in performing the x-ray measurements. This material is based on research sponsored by the Australian Research Council Future Fellowship Scheme (FT0990622), and the Air Force Research Laboratory under agreement number AOARD-10-4078.

High average power (11 W) eye-safe diamond Raman laser

Aaron McKay*, Ondrej Kitzler, Hua Liu, David Fell, Richard P. Mildren

MQ Photonics Research Centre, Dept. of Physics and Astronomy,
Macquarie University, Sydney, New South Wales 2109 Australia

ABSTRACT

We report external cavity Raman lasers using a 9.5-mm-long low-loss CVD diamond pumped by a 35 W q-switched Nd:YVO_4 laser with approximately 22 ns pulses at 36 kHz pulse repetition frequency. Two systems were investigated. The first demonstrated first and second Stokes simultaneously with more than 14.5 W of combined optical power. For an output coupler optimized for second Stokes only output (1485 nm), 11.1 W at 38% conversion efficiency was obtained. This output power is comparable to the maximum output powers reported for competing pulsed eye-safe technologies such as optical parametric oscillators and Er:YAG lasers.

Keywords: Diamond; Raman laser; High-power laser; Eye-safe laser; Stimulated Raman scattering; Q-switched lasers.

1. INTRODUCTION

Applications in the eye-safe wavelength region between 1400 and 1800 nm require convenient coherent sources with high average output power. There are a number of well-studied techniques for generating pulsed eye-safe output including optical parametric oscillators (OPOs) [1]-[3], selected solid-state lasers such as resonantly-pumped Er:YAG [4],[5], and those that employ a gas or solid-state Raman shifter [6]-[12]. Laser range finding, scanning lidar, and other remote sensing applications would benefit from power scaling of nanosecond-pulsed, high-average-power lasers beyond the 10 W level.

High energy eye-safe pulses have been generated using OPOs employing solid-state media such as KTP, KTA and BBO feature high conversion efficiencies (>40%), wide tunability and compact design. However for most OPOs, a pump laser with excellent beam quality is an important requirement which tends to limit performance. Webb et al. has previously demonstrated the high eye-safe average power of 33 W (although only at the relative slow pulse rates) with a KTA ring OPO [1]. This OPO, like many other high-average-power OPOs, had poor beam quality due to in part thermal issues arising in the non-linear crystal. More modest powers, for example 13.6 W and 3.6 W, have also been demonstrated with much higher repetition rates in intracavity OPOs; see respectively Dong et al.[2] and Zhu et al.[3].

Raman cells that use methane and deuterium mixtures have been demonstrated in lidar systems to shift 1064 nm radiation to 1543 nm [6], however these gas-based Raman shifters also often result in poor beam quality, limited repetition rates to a few hertz and frequent maintenance requirements. In addition, the combination of explosive gases and the strong possibility of laser-induced breakdown make gas Raman converters problematic for some practical applications.

Crystalline-based Raman shifters based on materials such as metal iodates, tungstates and vanadates have become an interesting approach for generating eye-safe radiation [7]. Since the typical Raman shift for crystals is approximately 1000 cm^{-1}, one of two approaches are typically applied: an efficient 1-μm pump laser and via cascade to the second or third Stokes [8],[9], or to use the typically weaker 1.3-μm emission from e.g., Nd-based lasers, with conversion to the first Stokes [10],[11]. Both these approaches have demonstrated good conversion efficiencies with average power levels in pulsed systems of up to ~5 W [10], but beyond this level have been limited by the availability of suitable pumping

* aaron.mckay@mq.edu.au; phone +61 2 9850 8975; fax +61 2 9850 8115; http://web.science.mq.edu.au/mqphotonics/

High-Power Lasers and Applications VI, edited by Upendra N. Singh, Dianyuan Fan, Jianquan Yao, Robert F. Walter, Proc. of SPIE Vol. 8551, 85510U · © 2012 SPIE
CCC code: 0277-786/12/$18 · doi: 10.1117/12.999857

sources and increasing thermal effects in the Raman crystals. In the former case, the Raman crystal bears a greater fraction of the system heat load.

Man-made diamond is a highly attractive laser material due to its exceptional material properties, which, in most cases outclass all competing materials [12]. Its high thermal conductivity, low thermal expansion (see for example Table 1), and wide transparency have already made diamond a popular material in high-power mid-IR lasers as windows and as heat spreaders in photonic and electronic high-end applications. In addition the Raman gain in diamond, comparable to that of barium nitrate at 1064 nm, makes diamond especially commendable for power scaling and wavelength conversion in high-power laser applications. Selected optical and thermal properties are compared for several more common Raman-active crystals with CVD-grown diamond in Table 1.

Table 1. Comparison of selected optical and thermal properties of popular Raman-active materials.

Crystal	Raman shift cm^{-1}	Raman gain cm/GW	Thermal conductivity W/m.K	Thermal expansion 10^{-6} m/K	dn/dT 10^{-6} K^{-1}	Damage threshold GW/cm^2
Diamond	1332	~10	~2000	1.1	20	~ 5
$Ba(NO_3)_2$ (BN)	1047	11	1.17	13	6	~ 0.4
$KGd(WO_4)_2$ (KGW)	768 901	4.4 3.3	2.5 to 3.4	1.6 to 8.5	-0.8 to -5.5	~ 10
$BaWO_4$ (BW)	924	8.5	3.0	6	<-9	~ 5
$SrWO_4$ (SW)	922	5.0	---	---	---	~ 5
YVO_4 (YV)	890	4.5	5.2	4.43	3 to 8.5	~ 1

In comparison to more mature Raman crystalline counterparts, diamond has already demonstrated the highest recorded first Stokes Raman output powers for both pulse [13] and continuous wave operation [14]. To the best of our knowledge, 12.3 W of Raman output power from approximately 170 W (~6.5% efficiency) represents the highest average power from any crystalline Raman laser [13]. This laser emitted from both end mirrors for a total output power of 24.5 W. In addition, when combined with well-established Nd laser technology, the 1332 cm^{-1} Raman frequency in diamond provides a convenient and efficient route to the eye-safe spectral region via its first [15], or second Stokes shift [16]. In the eye-safe spectral region, near 1.5 μm, the average output powers from crystalline Raman lasers, to-date, have typically been limited to several-watts of output power [15]-[17].

In this paper, we report a power scaled external cavity Raman laser which is based on the low-average power diamond Raman laser by Sabella et al. [16]. The Raman laser uses a 9.5-mm-long low-loss CVD diamond and lases on purely the second Stokes shifted line, near 1485 nm. The diamond Raman laser was pumped by a 35 W q-switched side-pump $Nd:YVO_4$ laser for more than 10 W of eye-safe Raman output. We also report efficient operation for 14.5 W device generating combined output at the first and second Stokes shifts at 1240 and 1485 nm.

2. PUMP LASER AND EXPERIMENTAL ARRANGEMENT

The optical arrangement of the external cavity Raman laser, including the pump module laser and subsequent isolator and polarization control, is shown in Figure 1. The pump laser produced approximately 35 W of polarized optical power to give an overall ~10% electrical-to-optical efficiency. The laser was q-switched using an acousto-optic modulator operating at ~35 kHz and produced 20±2 ns q-switched pulses. The peak power was ~47.5 kW. The pump power from the module laser was varied using a rotatable half waveplate and high-power optical isolator to ensure constant beam and pulse characteristics. Also a second half waveplate was used to align the polarization of the pump radiation to the <111> axis of the diamond to maximize the Raman gain in diamond [18].

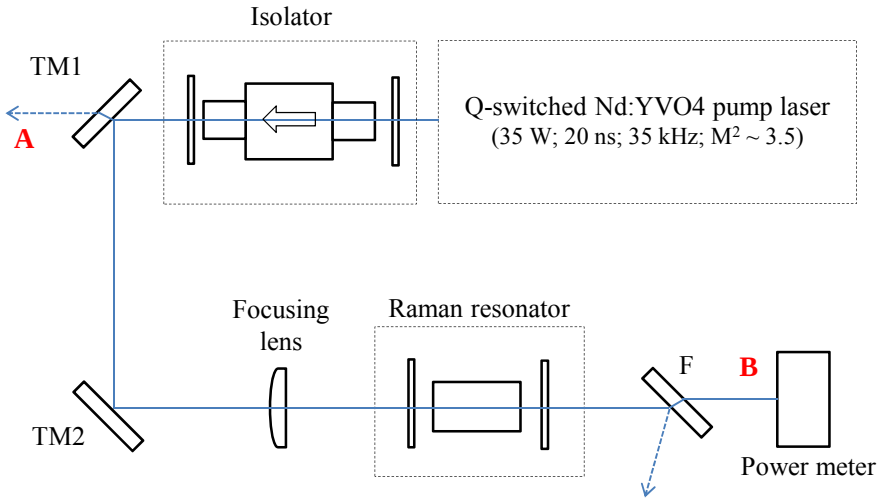

Figure 1. Experimental setup of diamond Raman laser and associated pump and isolator stages. Locations A and B refer to monitoring points of the pump pulse (A), and Raman output (B). TM1 and TM2 are turning mirrors with small amount of leakage (<<1%); F is an optional dichroic filter reflecting >99% of the pump.

A single spherical lens focused the pump beam into the diamond crystal so that the confocal parameter closely matched the diamond length. The diamond in this experiment was a 9.5-mm long, low-nitrogen content, ultra-low birefringence, Type IIa single crystal diamond grown by chemical vapor deposition ("Type IIIa" Element Six, UK). The propagation direction was along the <110> direction and end-faces were AR coated for 1240 nm.

3. COMBINED 1ST AND 2ND STOKES DIAMOND RAMAN LASER

The external cavity diamond Raman laser was formed by a planar input mirror and a 50-cm radius-of-curvature output mirror which gave calculated cold-cavity fundamental waists of 225 µm at 1240 nm and ~246 µm at 1485 nm. The physical resonator length was ~2 cm. The input mirrors were custom coated with high-damage threshold dielectric coatings which were 92% transmissive at 1064 nm and highly (>99.5%) reflective at the first three Stokes transmissions (i.e., 1240, 1485, and 1851 nm). Initially as an output coupler, we used a highly (>99.9%) reflective 1064-nm mirror with 18% transmission at the first Stokes shift at 1240 nm and transmissions at higher Stokes orders of less than 20%. The output coupler was highly reflective at the pump which allowed for a second pass of the pump through the Raman crystal to assist in raising conversion efficiency.

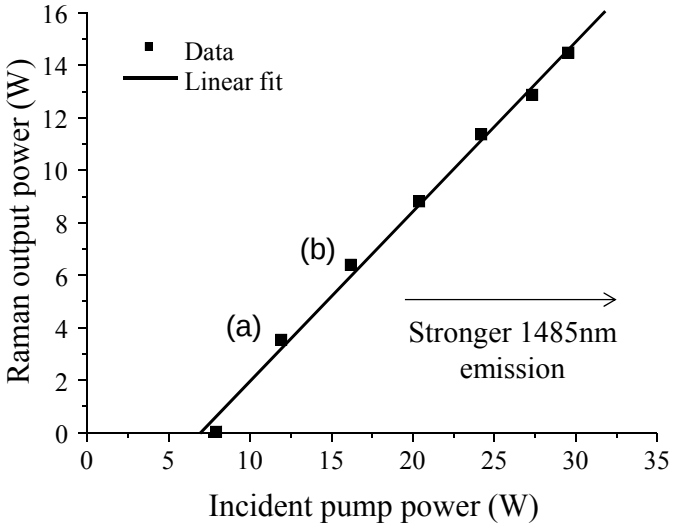

Figure 2. Combined 1st and 2nd Stokes output power as a function of incident pump power on diamond crystal.

The external cavity Raman laser produced more than 14.5 W of optical power as shown in Figure 2, measured using a calibrated optical power meter (Ophir FL250A). The slope efficiency well above threshold was 65% and the overall efficiency at maximum power was 50%. To the author's knowledge, the output power represents the highest for a crystal Raman laser and limited only by the available pump power. In comparison to the 170W-pumped system of Ref [13], the present device also offers an approximately 8 times improvement in efficiency due to the significantly reduced threshold and optimized single-ended output mirrors.

The output spectrum consisted of first and second Stokes radiation at 1240 and 1485 nm respectively. Using an uncalibrated CCD-based spectrometer (Ocean Optics NIR512) we estimate at the operating point (a) in Figure 2 approximately 80% of power is first Stokes, and at the operating point (b) the power is shared equally between the first two Stokes. Only at very low powers (< 2 W) did this resonator lase only at the first Stokes. At maximum output power, 14.5 W of the radiation was cascaded into the second Stokes field at 1485 nm. No third Stokes output was observed.

4. HIGH-POWER EYE-SAFE DIAMOND RAMAN LASER

A second external cavity diamond Raman laser was built using the same pump and polarization control arrangement as depicted in Figure 1 except using an output coupler design to enhance the cascade to the second Stokes. The output coupler was highly reflective at the first Stokes, and had approximately 85% transmission at the desired second Stokes order which previous studies has shown is near optimal output coupling for second Stokes output [16]. The transmission spectra, obtained using a Cary 5000 spectrophotometer, for the input and output mirror are given in Figure 3. (The input mirror was retained from the previous laser.)

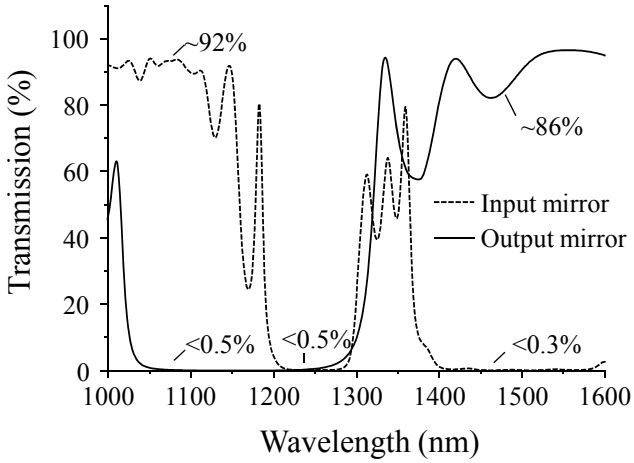

Figure 3. Transmission spectra for the input and output mirrors of the eye-safe diamond Raman lasers.

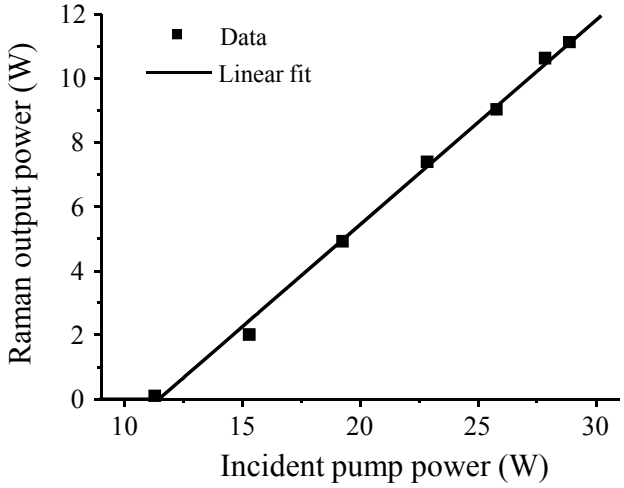

Figure 4. Raman output power for an eye-safe diamond Raman laser as a function of pump power incident on diamond crystal.

As shown in Figure 4, the diamond Raman laser produced 11.1 W of 1485 nm radiation which represents a six-fold increase in average-power compared to Ref [16]. The slope efficiency of the laser was 60% with overall efficiency of 38%.

The high-reflectivity dichroic filter, F in Figure 1, was replaced with a dichroic filter with high reflectivity at the pump and first Stokes wavelengths. The reflected residual first Stokes from the dichroic mirror was less than the specified power noise level of the power meter. The optical spectrum, in absence of the dichroic mirror, was also used to confirm sole second Stokes operation. The spectrum was determined using a fiber-coupled infrared scanning spectrometer (Band House Design, SIR2600) with a spectral response between 1.0 and 2.6 μm. The spectrum revealed an instrument-limited (~1.3-nm half-width-half-maximum bandwidth) 1485-nm signal. The contrast between this second Stokes intensity and the first Stokes was greater than $\sim 2.5 \times 10^3$. This level of contrast between desired and suppressed Stokes orders remained constant at all measured power levels.

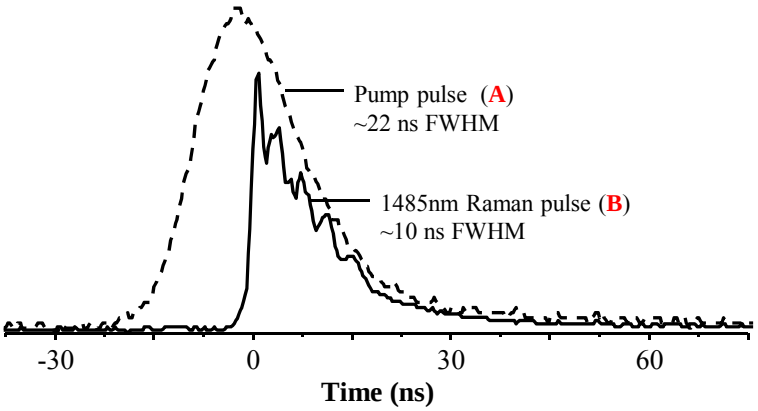

Figure 5. Typical temporal characteristics of the pump (dotted), residual (dashed), and Raman (solid lines) output pulses traces demonstrating efficient conversion of pump pulses. Pulses were measured at locations indicated in Figure 1.

Figure 5 shows typical temporal characteristics of the pump and Raman outputs, recorded at the ~10 W output power level. The pulse shapes were measured using a ~500 MHz-bandwidth Si and a 1 GHz-bandwidth InGaAs photodiodes located at A and B respectively in Figure 1 and were recorded using an digital oscilloscope (Agilent DSO-X 3043A: 350 MHz; 4 GSa/s). These temporal characteristics of the pump, residual pump and Raman pulse shapes as shown in Figure 5 demonstrate excellent Raman conversion once threshold is surpassed at times approximately 10 ns after the leading edge of the pump pulse.

5. DISCUSSIONS AND CONCLUSIONS

Table 2. Comparison of leading laser technologies for generating high-average power eye-safe radiation.

	Technology	Average Power	Pulse Repetition Frequency	Efficiency	Reference
High PRF	Raman extra-cavity diamond	11.1 W	35 kHz	40%	This work
	OPO (high pulse rate)	13.6 W	18 kHz	5.7%	[2]
	Resonantly pumped Er:YAG	9.5 W	10 kHz	49%	[4]
	Self-Raman lasers	5.2 W	20 kHz	20%	[10]
Low PRF	OPO low pulse rates	33 W	100 Hz	35%	[1]
	Raman gas cells	17.5 W	50 Hz	43%	[6]

Table 2 shows a comparison of completing laser technologies for generating eye-safe radiation at high-average powers. Compared to molecular ion crystal Raman lasers, diamond has enabled a doubling of the overall efficiency and output powers. Compared to OPOs, the present diamond system has achieved similar average power levels but with much higher conversion efficiency from the pump laser. Since the output powers demonstrated in this work was only limited by the available pump power, and due to the excellent thermal properties of diamond, higher average power eye-safe lasers based on Raman conversion in diamond are likely in the near future.

In summary, we have shown that pulsed Raman laser power levels greater than 10 W can be readily achieved using diamond with efficiency much higher than previously obtained in other crystals. Spectrally pure output with ~11.2 W has been demonstrated at 35 kHz in the eye-safe region near 1485 nm—a 6-fold increase from a previously reported eye-safe diamond Raman laser. A combined first and second Stokes external cavity diamond laser has also yielded record power levels of 14.5 W and overall efficiencies of 50%. We have shown that the efficiency routinely seen at low power levels is sustainable at powers above 10 W. As a result, diamond Raman laser technology is promising for a range of efficient and high-average power lasers in the near infrared at their harmonic wavelengths.

ACKNOWLEDGMENTS

The authors thank Alex Sabella for his expert advice during the project design. This material is partly based on research sponsored by the Australian Research Council Future Fellowship Scheme (FT0990622), and the Air Force Research Laboratory under agreement number AOARD-10-4078 and AOARD-12-4055.

REFERENCES

[1] Webb M. S., Moulton P. F., Kasinski J. J., Burnham R. L., Loiacono G., and Stolzenberger R., "High-average-power $KTiOAsO_4$ optical parametric oscillator," Optics Letters, **23**, 1161-1163 (1998).

[2] Dong X.-L., Zhang B.-T., He J.-L., Huang H.-T., Yang K.-J., Xu J.-L., Zuo C.-H., Zhao S., Qiu G., and Liu Z.-K., "High-power 1.5 and 3.4 μm intracavity KTA OPO driven by a diode-pumped Q-switched Nd:YAG laser," Optics Communication, **282**, 1668-1670 (2009).

[3] Zhu H., Zhang G., Chen H., Huang C., Wei Y., Duan Y., Huang Y., Wang H., and Qiu G., "High-efficiency intracavity Nd:YVO4\KTA optical parametric oscillator with 3.6 W output power at 1.53 μm," Optics Express **17**, 20669-20674 (2009).

[4] Setzler S. D., Francis M. P., Young Y. E., Konves J. R, and Chicklis E. P., "Resonantly pumped eyesafe erbium laser," IEEE Journal of Selected Topics in Quantum Electronics **11**, 645-657 (2005).

[5] Bigotta S., and Eichhorn M., "Q-switched resonantly diode-pumped Er^{3+}:YAG laser with fiber like geometry," Optics Letters **35**, 2970-2972 (2010).

[6] Spuler S. M., and Mayor S. D., "Raman shifter optimized for lidar at a 1.5 μm wavelength," Applied Optics **46**, 2990-2995 (2007).

[7] Basiev T. T., Osiko V. V., Prokhorov A. M., Dianov E. M., [Solid-State Mid-Infrared Laser Sources], Springer Berlin Heidelberg, Ch 8 (2003).

[8] Lisinetskii V.A., Eichler H.J., Rhee H., Wang X., and Orlovich V.A., "The generation of high pulse and average power radiation in eye-safe spectral region by the third stokes generation in barium nitrate Raman laser," Optics Communication, **281**, 2227-2232 (2008).

[9] Lisinetskii V. A., Riesbeck T., Rhee H., Eichler H. J., and Orlovich V. A., "High average power generation in barium nitrate Raman laser, " Applied Physics B **99**, 127-134 (2010).

[10] Chen X. H., Zhang X. Y., Wang Q. P., Li P., Liu Z. J., Cong Z. H., Li L., and Zhang H. J., "Highly efficient double-ended diffusion-bonded Nd:YVO_4 1525-nm eye-safe Raman laser under direct 880-nm pumping," Applied Physics B **106**, 653-656 (2012).

[11] Zong N., Cui Q., Ma Q., Zhang X., Lu Y., Li C., Cui D., Xu Z., Zhang H., and Wang J., "High average power 1.5 μm eye-safe Raman shifting in $BaWO_4$ crystals," Applied Optics **48**, 7-10 (2009).

[12] Mildren R. P., Butler J. E., and Rabeau J. R., "CVD-diamond external cavity Raman laser at 573 nm," Optics Express **16**, 18950-18955 (2008).

[13] Feve J.-P. M., Shortoff K. E., Bohn M. J., and Brasseur J. K., "High average power diamond Raman laser," Optics Express **19**, 913-922 (2011).

[14] Kitzler O., McKay A., and Mildren R. P., "Continuous-wave wavelength conversion for high-power applications using an external cavity diamond Raman laser," Optics Letters **37**, 2790-2792 (2012).
[15] Jelínek M., Kitzler O., Jelínková H., Šulc J., and Němec M., "CVD-diamond external cavity nanosecond Raman laser operating at 1.63 μm pumped by 1.34 μm Nd:YAP laser," Laser Physics Letters, **9**, 35-38 (2012).
[16] Sabella A., Piper J. A., and Mildren R. P., "Efficient conversion of a 1.064 μm Nd:YAG laser to the eye-safe region using a diamond Raman laser," Optics Express **19**, 23554-23560 (2011).
[17] Fan Y. X., Liu Y., Duan Y. H., Wang Q., Fan L., Wang H. T., Jia G. H., and Tu C. Y., "High-efficiency eye-safe intracavity Raman laser at 1531 nm with $SrWO_4$ crystal," Applied Physics B, **93**, 327-330 (2008).
[18] Sabella A., Piper J. A., Mildren R. P., "1240 nm diamond Raman laser operating near the quantum limit," Optics Letters **35**, 3874-3876 (2010).